Superfluid critical behavior in the presence of a dilute correlated impurity

G. K. S. Wong,* P. A. Crowell, H. A. Cho, and J. D. Reppy
The Laboratory of Atomic and Solid State Physics and the Material Sciences Center, Clark Hall, Cornell University, Ithaca, New York 14853-2501
(Received 3 September 1992)

Measurements of the superfluid density and heat capacity in porous aerogel glasses that are *completely filled* with liquid helium are presented as examples of critical behavior in the presence of a dilute correlated impurity. Longstanding doubts about the existence of critical behavior in ^{4}He-filled porous media, brought about by the failure of all previous searches for a singularity in anything other than the superfluid density, are put to rest by the observation of a sharp heat-capacity singularity that is coincident with the superfluid transition. With the notable exception of the superfluid transition in pure helium itself, the superfluid transitions in ^{4}He-filled aerogel are among the sharpest phase transitions ever seen. However, the critical exponents for the superfluid density and heat capacity are both markedly different from the corresponding exponents in pure helium. We conclude that the correlated disorder introduced by the aerogel glass drives this system away from the three-dimensional XY universality class to which pure helium belongs.

I. INTRODUCTION

The most stringent experimental tests of the theories of critical phenomena have always come from studies of the superfluid phase transition in liquid ^{4}He because this transition is, by at least two to three orders of magnitude, the sharpest phase transition ever seen.[1] This work reached its apogee in the remarkable agreement between the critical exponent measurements of Ahlers and coworkers[2] and the renormalization group (RG) theories of Wilson and others.[3,4] However, outstanding issues remain. One of them is the effect of the disorder that is introduced by sample inhomogeneities and its connection to the rounding that is observed in any real phase transition.[5] Seminal considerations of disorder by Harris and others[6,7] concluded that, in the absence of long-range correlations, rounding would not appear. However, a new set of critical exponents would appear in the impure system if the specific heat exponent of the pure system was positive. Experiments on randomly diluted Ising antiferromagnets[8] have generally supported the Harris predictions, under the somewhat less stringent criteria mandated by the lack of a magnetic system with a phase transition that is as sharp as the one seen in superfluid helium. Although there is a general belief that rounding has something to do with long-range correlated disorder, relatively little work has been done to delineate those conditions under which correlated disorder might lead to a rounded as opposed to a sharp phase transition. In the latter case, one would also like to know what the critical exponents might be. Weinrib and Halperin[9] have addressed this issue theoretically, but recent experiments on helium in porous media[10,11] have uncovered many inadequacies in our understanding of such systems.

This paper is a review of our experiments on the critical behavior of both the superfluid density and the heat capacity in two different ^{4}He-filled aerogels.[12] In all cases, the aerogel pores were *completely filled* with liquid helium. The thin film situation will not be discussed in this paper. We will begin with a quick review of the theoretical notation used in the study of critical phenomena at the superfluid phase transition and a summary of the existing theories of disorder in critical phenomena. The focus of the work on helium in porous media has evolved significantly over the years and so we will discuss the experimental background from a historical perspective.

A. Theoretical background

1. *Critical phenomena at the λ transition*

Good general introductions to scaling, universality, and the renormalization group theory of critical phenomena can be found in the review articles by Fisher and by Kadanoff.[4] On the experimental side, the reviews by Ahlers[2] serve as a good introduction to the superfluid phase transition.

Existing theories of critical phenomena are generally restricted to statements about the asymptotic behavior very close to the phase transition, which is at $T_c = 2.172$ K for superfluid ^{4}He. The independent variable of choice is the *reduced temperature,*

$$t = T/T_c - 1 \ , \tag{1}$$

and the quality of an experiment, or implicitly, the quality of the particular sample that is measured, is judged by how close to the transition one is able to take meaningful data. In other words, what is the smallest measured $|t|$ on a logarithmic scale? Very close to the transition, in the limit $t \to 0$, the superfluid density $\rho_s(t)$ and the heat capacity $C(t)$ approach the asymptotic power laws

$$\rho_s(t) \sim \rho_{s_0} |t|^{\zeta} \quad \text{for } t < 0 \tag{2}$$

and

$$C(t)\sim \begin{Bmatrix} \frac{A}{\alpha}|t|^{-\alpha} & \text{for } t>0 \\ \frac{A'}{\alpha}|t|^{-\alpha} & \text{for } t<0 \end{Bmatrix} + \text{analytic background} . \tag{3}$$

The parameters ζ and α are called the *critical exponents,* whereas the parameters ρ_{s_0}, A, and A' are called the *critical amplitudes.* Critical exponents are universal in that they depend only on the dimensionality d of the system and the number of components n in the order parameter. In particular, superfluid ^{4}He belongs to the universality class $d=3$ and $n=2$, called the three-dimensional XY model. The best number for ζ is based on the second-sound measurements of Greywall and Ahlers.[13,14] The best number for α is based on the heat-capacity measurements of Ahlers[15,14] and, more recently, Lipa and Chui.[1]

$$\zeta=0.6717\pm0.0004 , \tag{4}$$

$$\rho_{s_0}=0.351 \text{ g/cm}^3 , \tag{5}$$

$$\alpha=-0.013\pm0.003 , \tag{6}$$

$$A=6.108 \text{ J/K mole} , \tag{7}$$

$$A'=5.771 \text{ J/K mole} . \tag{8}$$

Since ζ is so close to $\frac{2}{3}$, the superfluid density is often said to follow a $\frac{2}{3}$ power law. Similarly, since α is so close to zero, the heat capacity is often said to have a logarithmic singularity. The best theoretical estimates for the critical exponents are based on the Borel-resummation technique of Le Guillou and Zinn-Justin.[16] They predict $\zeta=0.672\pm0.002$ and $\alpha=-0.016\pm0.006$, both in good agreement with the experimental data.

Universality exists because, close to the transition, the physics is dominated by the large-scale fluctuations of the order parameter, not by the small-scale structure of the system under study. These fluctuations occur on *all* length scales up to the *correlation length* $\xi(t)$, which diverges as $t\to0$ with another power law,

$$\xi(t)\sim \begin{cases} \xi_0|t|^{-\nu} & \text{for } t>0 \\ \xi_0'|t|^{-\nu} & \text{for } t<0 . \end{cases} \tag{9}$$

Strictly speaking, for isotropic systems with two or more components in the order parameter, standard definitions of the correlation length yield infinity at *all* temperatures less than T_c, and the quantity that is generally identified as ξ in these situations is the *phase coherence length.*[17,18] This length scale can be derived from considerations of the helicity modulus (the free energy associated with a twisting of the phase of the order parameter), which leads to the relation

$$\xi(t)=\left[\left[\frac{k_B T m^2}{\hbar^2}\right]\frac{1}{\rho_s(t)}\right]^{1/(d-2)} . \tag{10}$$

Using the published data for ρ_s, we compute $\xi_0'=0.344$ nm.

In general, critical exponents within the same universality class obey a variety of scaling relations. The superfluid density and correlation length exponents are related through $\zeta=(d-2)\nu$. The appearance of the dimensionality d in this relation is symptomatic of the fact that *hyperscaling* had to be assumed at some point in the derivation. Hyperscaling relations are those that connect thermodynamic quantities with the critical point fluctuations. A good example is the relation between the heat-capacity and correlation length exponents, $d\nu=2-\alpha$. Most useful for us is the relation that connects the superfluid density exponent with the heat-capacity exponent,

$$d\zeta=(d-2)(2-\alpha) . \tag{11}$$

There are also universal relations between the critical amplitudes. Hyperuniversality,[19] which used to be called two-scale-factor universality, connects the heat capacity *per unit volume* to the superfluid *mass* density via a dimensionless universal number X. It is equivalent to asserting that the singular part of the free energy inside a hypercube with linear dimensions equal to the correlation length is a temperature-independent universal number. This dimensionless number, which is 0.62 in the case of superfluid helium, is defined as

$$X=\frac{1}{k_B}\alpha t^2 C(t)\left[\frac{k_B T m^2}{\hbar^2\rho_s(t)}\right]^{d/(d-2)} . \tag{12}$$

Phase transitions in real systems are rounded,[5] meaning that power-law behavior is never observed at the smallest values of t. For magnetic phase transitions in solid systems, defects and impurities limit the sharpness of the phase transition to 10^{-4} at best, 10^{-3} more typically. At liquid-vapor critical points, the fluid compressibility diverges and, therefore, all experiments done under the earth's gravitation field have had problems with concentration gradients. Transitions as sharp as 10^{-4} to 10^{-5} have been observed, but only by stirring the fluid and/or somehow correcting for the concentration gradients. The most precise tests of the RG theory of critical phenomena have come from studies of superfluid ^{4}He. Transitions as sharp as 10^{-8} have been observed by Lipa and Chui,[1] as the pressure dependence of the λ point is so weak that, under the earth's gravitation field, the transition temperature gradient is only 1.194 μK/cm.

2. *Disorder effects in critical phenomena*

This discussion will be couched in the language of magnetic phase transitions. The applicability of studies on magnetic systems to superfluid helium is due to the existence of universality in critical phenomena. A recent review of disorder in critical phenomena was published by Grinstein.[20]

Our objective was to study the effect of disorder introduced by the addition of a *quenched* impurity, aerogel glass, to an otherwise ideal system, liquid ^{4}He. In contrast, ^{3}He dissolved in liquid ^{4}He is said to be an annealed impurity because the impurity atoms are not fixed in space. Quenched impurities in magnetic systems fall into one of two categories. In the first case, called random exchange disorder, nonmagnetic impurities in the sample

lead to spatial inhomogeneities in the locally averaged strength of the magnetic interaction. Since the transition temperature depends on the strength of these averaged interactions, random exchange disorder is often modeled as a distribution of *locally* defined transition temperatures, $T_c(\mathbf{r})$. The second category, which is not the subject of this paper, is called spin-glass disorder. It corresponds to the case in which the sign of the magnetic interaction, not just the magnitude, is made to vary from point to point.

Much of the RG theoretical infrastructure in critical phenomena was developed for *ideal* systems, macroscopically homogeneous and infinite in extent. The first exactly solved model of a disordered phase transition was the two-dimensional (2D) disordered Ising model of McCoy and Wu.[21] In this model, the perfectly ordered rectangular lattice was preserved and all horizontal interactions were the same. The vertical interactions were independent of column but varied randomly from row to row. McCoy and Wu's solution was very striking because all of the critical point singularities were smeared out. At that time, a disordered system was often modeled as a weighted average of an ensemble of independent and sharp phase transitions with a distribution of T_c's. This approach also gave smeared transitions. Coupled with the observation of smearing in all real phase transitions, these ideas led many people to associate smearing with disorder or inhomogeneity.

The relation between disorder and rounding, however, is more subtle. This first became apparent when Harris[6] showed that disorder does not necessarily lead to rounding. He considered only homogeneously disordered systems, ones in which the local impurity concentration is uniform across the sample when averaged over a sufficiently large volume. Therefore fluctuations in the local T_c, defined over independent volume elements of size ξ^d, would be expected to go to zero as $\xi \to \infty$. Adopting a self-consistent approach, he argued that such a system would be stable against the smearing effects of disorder if the fluctuations in the local T_c decayed to zero faster than $|T-T_c|$ as $\xi \to \infty$. The fluctuations in the local impurity concentration were assumed to follow a Poisson distribution, so that the local T_c fluctuations scaled as $\delta T_c/T_c \sim \xi^{-d/2}$. This stability criterion, now named after Harris, was written in terms of the critical exponents for the pure undiluted system:

$$2-d\nu_{\text{pure}}=\alpha_{\text{pure}}<0 \ . \tag{13}$$

Pure systems that satisfied this criterion would, after impurity dilution, undergo sharp phase transitions with the *same* critical exponents as the undiluted system. Harris suggested that $\alpha_{\text{pure}}>0$ would lead to smearing, but subsequent RG calculations[7] revealed that a sharp phase transition with a new set of critical exponents would result instead. A very important feature of these new exponents was that α_{impure} was strictly negative. So, the new exponents were stable against further applications of the Harris argument. This prediction has generally been confirmed by experiments on randomly diluted 3D Ising antiferromagnets,[8] where the pure system exponent $\alpha_{\text{pure}}=0.11$ is positive.

To reconcile the Harris result with the observation of rounding in all real systems, one has to consider *correlated* disorder. This results from impurities that are not homogeneously distributed on any experimentally achievable length scale. Certainly, the model of McCoy and Wu had correlated disorder. An explicit RG calculation was developed by Weinrib and Halperin.[9] They considered a particular distribution of local T_c whose spatial correlations decayed to zero with a power law,

$$\langle T_c(\mathbf{0})T_c(\mathbf{r})\rangle \sim r^{-a} \ , \tag{14}$$

as $r \to \infty$. When the correlations decayed fast enough, $a>d$, the Harris criterion for short-range or uncorrelated disorder was recovered. In the case of long-range correlated disorder, $a<d$, an extended Harris stability criterion was derived,

$$2-a\nu_{\text{pure}}<0 \ . \tag{15}$$

A new set of critical exponents was predicted for those situations in which this extended Harris criterion was violated. Weinrib and Halperin argued that the correlation length exponent for these impure systems would satisfy a simple relation,

$$\nu_{\text{impure}}=2/a \ , \tag{16}$$

which they believed to be exact. The salient observation was that, for $a<2$, the superfluid density exponent of $\zeta=\nu>1$ could be interpreted as a smeared transition. Thus, at least in principle, this theory quantified the oft-used statement "macroscopic inhomogeneities lead to smearing."

There is, however, one situation admitted by Weinrib and Halperin's theory that was never observed. In 3D, there is a narrow range of decay exponents, $2<a<3$, for which sharp phase transitions with new critical exponents are expected. To be truly convincing, any demonstration of this effect has to be done on a system that is stable against the type of disorder considered by the Harris argument. Superfluid helium is a candidate for the pure system because its heat-capacity exponent is negative, albeit, only slightly so. Aerogel glass is interesting in this regard because it is known to have long-range correlations.[22,23] As it turned out, none of the existing theories is able to describe our ^{4}He-filled aerogels. We will discuss why in our final section.

B. Experimental background

The earliest experiments on ^{4}He-filled porous media were conceived as part of an effort to study finite-size confinement effects. These experiments showed a continuous depression of the superfluid transition temperature T_c with decreasing pore size.[24] The theoretical explanation given for this effect was the *healing length* concept of Ginzburg, Pitaevskii, and Mamaladze.[25] One assumed that the superfluid density was zero at the boundary and that it grew back to its bulk value over a healing length $l(T)$ given phenomenologically by

$$l(T)=l_0(1-T/T_\lambda)^{-2/3} \ , \tag{17}$$

with l_0 typically of order 0.4 nm. The macroscopic superfluid density would appear to go to zero when $l(T)$ became comparable to the pore size D, leading to a depression in the superfluid transition temperature of the form

$$(1-T_c/T_\lambda)\sim(D/l_0)^{-3/2}\ , \tag{18}$$

give or take a geometry-dependent dimensionless scale factor. It was essential in this theory that $l(T)$ continued to diverge at T_λ, even though the apparent superfluid density went to zero at T_c. In other words, the healing length picture presumed that there was not a real phase transition at T_c. Although these ideas have now been superseded by the renormalization group picture, we note that modern RG theories of finite-size confinement, such as the work of Huhn and Dohm,[26] do in fact assume Dirichlet boundary conditions that are vaguely reminiscent of the healing length picture.

The inadequacies of the healing length picture were first demonstrated by measurements of the superfluid density in ^{4}He-filled Vycor. Reppy and co-workers[27] found that these data obeyed the $\frac{2}{3}$ power law that was expected from universality arguments for any 3D body of superfluid helium. They proposed that there really was a phase transition at T_c, with a divergent correlation length inversely proportional to the superfluid density. Once this correlation length grew much larger than the pore size, the critical behavior would be governed only by the long-range 3D connectivity of the porous structure. This structure might alter the scale of the measured parameters, but it would not change the essential nature of the phase transition, meaning that 3D interconnected porous media were really not very good systems in which to study purely finite-size effects. Had the Vycor data not existed, these arguments would have been dismissed as circular because the existence of a divergent correlation length had to be assumed in order to prove its relevance close to T_c. However, these data were consistent with the correlation length arguments and, in time, even moderately thin films of ^{4}He confined to the surface of Vycor glass were shown to obey the $\frac{2}{3}$ power law.

Many questions and doubts were raised by this interpretation. The first was that superfluid power laws in ^{4}He-filled Vycor were limited to only one and a half decades of reduced temperature, with a pronounced rounding starting at $10^{-2.5}$. This put a limit on how accurately the exponent, $\zeta=0.67\pm0.03$, could be determined as the transition temperature had to be chosen to give the best possible power-law fit. Furthermore, subsequent attempts[28,29] to observe the heat-capacity singularity that was supposed to be associated with this phase transition all met with failure. As we show in Fig. 1, the heat capacity had only a broad maximum at a temperature somewhat larger than T_c, which was qualitatively consistent with finite-size expectations. Although there were theoretical arguments based on hyperuniversality that predicted that the critical point fluctuation contribution to the heat-capacity singularity would be too small to be measured in the Vycor system, the arguments were suspect because they had to assume that there was a real phase transition at T_c.

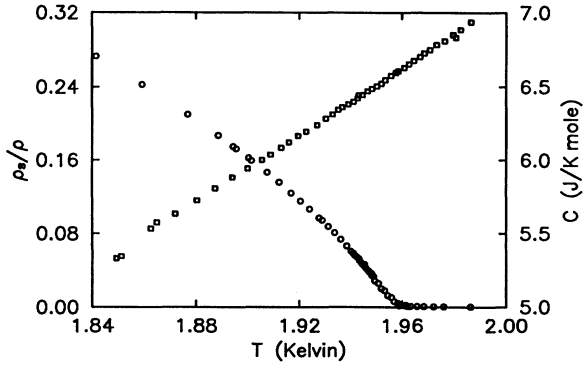

FIG. 1. To emphasize the lack of a coincident heat-capacity singularity in ^{4}He-filled Vycor, we plot the superfluid density data (○) of Chan *et al.* (Ref. 10) alongside the heat-capacity data (□) of Finotello *et al.* (Ref. 29). The scatter in the heat-capacity data is 0.1% and the maximum in the heat capacity occurs at 2.1 K, off the scale of this plot.

In 1987, we obtained a new type of porous medium, a *densified* xerogel glass.[30] Torsional oscillator measurements by Chan *et al.*[10] revealed a superfluid density power law that was clearly not $\frac{2}{3}$, as shown in Fig. 2. This suggested that the results obtained earlier for ^{4}He-filled Vycor were not universal and it weakened the case for a full three-dimensional phase transition at T_c. We thus chose to address the finite-size issue directly by selecting a porous medium with a wide distribution of pore sizes, one for which simple finite-size considerations would predict a severely broadened transition. The selected medium was aerogel glass, which, although similar to xerogel in some aspects of its production, was especially noted for its lack of a well-defined pore size. The aerogel superfluid density measurements of Chan *et al.*[10] also did not show a $\frac{2}{3}$ power law, but they did uncover the sharpest phase transitions that had ever been seen in any ^{4}He-filled porous media. These power laws extended down to $10^{-4.3}$ in reduced temperature, well over an or-

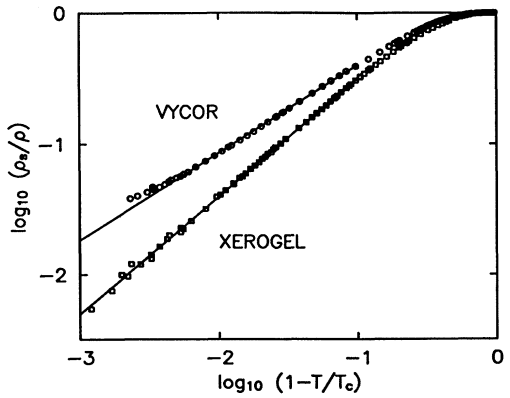

FIG. 2. The superfluid density power laws for ^{4}He-filled Vycor (○) and ^{4}He-filled xerogel (□) have exponents ζ equal to 0.67 ± 0.03 and 0.90 ± 0.02, respectively, based on the torsional oscillator measurements of Chan *et al.* (Ref. 10).

der of magnitude improvement on the Vycor and xerogel results, and in complete disagreement with simple finite-size considerations.

To understand the differences in the superfluid properties, we looked into the differences in the physical structure of our various porous media. Aerogels are noted for their exceedingly high porosities or, in a related sense, their extremely low densities. Our first samples had a porosity of 93.9%, so that, once filled with helium, the ^{4}He-filled aerogel system was like a large body of liquid in the midst of a 6.1% volume impurity. In contrast, the Vycor and xerogel samples had porosities of 30% and 60%, respectively. The small T_c shifts that we observed, 4.0–5.7 mK for the first set of aerogels, were less than 3×10^{-3} of the pure system transition temperature, which meant that we were in a *dilute* regime. For comparison, the Vycor and xerogel samples induced T_c shifts of 220 and 84 mK, respectively. Most important of all, aerogel glass is known from both theory and experiment to be exceptionally nonuniform, with highly ramified structures extending over a wide range of length scales.[22,23] Vycor, in contrast, does not have such long-range correlated structures. Armed with our knowledge of disorder effects in critical phenomena, we attributed these new exponents to the long-range correlated disorder that we knew to be present, even though we could not actually derive the exponents from the scattering data.

In any case, there was still one major piece of missing evidence. Although Finotello, Gillis, Wong, and Chan[29] did observe singularities in the heat capacity of thin ^{4}He films adsorbed on the surface of Vycor and xerogel, their singularities disappeared when the pores were completely filled with liquid helium. The existence of this heat-capacity singularity is particularly significant because, together with the lack of a latent heat, it is almost the defining characteristic of a continuous phase transition. One notable exception is the Kosterlitz-Thouless transition for two-dimensional ^{4}He films,[31] for which the heat capacity has only an essential singularity, with finite derivatives to all orders in T. Significantly, our heat-capacity experiments on ^{4}He-filled aerogel revealed the presence of a sharp singularity in the heat capacity that is *coincident* with the superfluid transition. This cusplike singularity is different from the logarithmiclike singularity that is seen in bulk helium, but it is consistent with our observation that the superfluid density critical behavior is not bulklike.

II. AEROGELS

A recent and comprehensive source of information on aerogels is the proceedings book edited by Fricke.[12] At a more elementary level, there is also an article by Fricke in the May 1988 issue of Scientific American.

A. Manufacture and handling of aerogels

All of our original experiments were conducted on an old block of aerogel donated to us by DESY, but manufactured by Airglass.[32] Our more recent experiments were done on a fresh block of aerogel purchased directly from Airglass. These aerogels were prepared in the traditional manner first developed by Nicolaon and Teichner:[33]

$$\mathrm{Si(OCH_3)_4+4H_2O\rightarrow Si(OH)_4+4CH_3OH}\ , \tag{19}$$

$$n\mathrm{Si(OH)_4\rightarrow[SiO_2]}_n+2n\mathrm{H_2O}\ . \tag{20}$$

In the first step, tetramethoxysilane (TMOS) is decomposed into $Si(OH)_4$ and methanol. $Si(OH)_4$ is not stable and it polymerizes very readily into colloidal aggregates of SiO_2, releasing water in the process, as indicated by the second equation. The result is a silica mesh immersed in methanol. Its density can be reduced by dilution with methanol. The reaction rate is usually accelerated by adding ammonia to increase the pH. Removal of the methanol solvent is done through a supercritical drying process, which prevents the formation of the liquid-vapor interface whose surface tension would otherwise crush the delicate silica gel structure.

Our aerogel samples were machined into cylinders, to a 0.025-mm tolerance, using an abrasive cutter. In our earliest runs, samples A–E, the cylinders were compressed into the sample holder using a taper. In our later runs, samples F and G, the cylinders were glued in place and no compression was used. The special epoxy that made this possible is called BIPAX Tra-Bond BA-2151.[34] As shown in Table I, the compressed samples exhibited a significant variation in T_c, even though they were cut from the same block of aerogel. The shift in the superfluid transition temperature, relative to the λ point, scaled monotonically with the degree of compression. In contrast, the T_c's for our two glued samples agreed to within the accuracy of our thermometers. We have opened up some of our cells after a liquid-helium experiment, examined the aerogel visually, and found it to be

TABLE I. For each run, we have listed the aerogel source and density, the sample diameter and height (after compression), the volume compression, the T_c shift, and the type of data taken.

Sample	Source	ρ (g/cm^3)	d (inch)	h (inch)	dV/V (%)	$T_\lambda-T_c$ (mK)	Data
A	DESY	0.133	0.250	<0.250	>5.4	5.66	ρ_s
B	DESY	0.133	0.257	0.265	8.0	5.23	ρ_s
C	DESY	0.133	0.366	0.117	7.1	4.50	C
D	DESY	0.133	0.740	0.102	1.1	4.00	C
E	DESY	0.133	0.252	0.265	3.4	4.34	both
F	Airglass	0.200	0.222	0.204	glued	7.01	ρ_s
G	Airglass	0.200	0.740	0.102	glued	7.10	C

intact. Evidently, the surface tension of liquid ^{4}He is not large enough to destroy the delicate aerogel structure.

B. Characterization on many length scales

Our DESY aerogel had a density of 0.133 ± 0.009 g/cm^3. The porosity deduced from a filling experiment on sample B was 93.7%, which is comparable to the 93.9% figure that we computed by assuming a density of 2.19 g/cm^3 for *amorphous* silica.[35] According to Airglass, the aerogel sample that we purchased directly from them had an optical index of refraction $n=1.042$. We computed the density ρ by using the empirical relation of Poelz and Riethmüller[36] and Henning and Svensson,[37]

$$\rho=\frac{n-1}{(0.210\pm0.002)}\ \text{g/cm}^3\ . \tag{21}$$

This gave us a density of 0.200 g/cm^3 for the Airglass aerogel, from which we deduced that the porosity was 90.9%.

Schuck and Dietrich[38] have performed a series of nitrogen adsorption-desorption isotherms on three samples of aerogel, from Airglass, with densities of 0.105, 0.145, and 0.275 g/cm^3. The specific surface areas were 625, 840, and 665 m^2/g, respectively. They did not explain why the surface areas were not monotonically related to the densities. The pore size distribution extended from the nm to the μm range, with mesopores of diameters up to 60 nm taking 13%, 25%, and 57%, respectively, of the total pore volume. Macropores larger than 60 nm comprised the majority of the pore volume, especially in the least dense aerogels. Exposure to ambient humidity did not change the macroscopic appearance of the aerogel, nor did it change the specific area by more than 5%, but it did collapse some of the larger mesopores and leave in its place a more narrow mesopore distribution centered around 15 nm. The DESY aerogel samples given to us were available partly because they were known to have been exposed to a damp environment while at DESY. In contrast, the Airglass samples were purchased fresh and kept in a dessicator at all times. To emphasize the total lack of a well-defined pore size, we have reproduced in Fig. 3 the aerogel TEM image of Tewari, Hunt, Lieber, and Lofftus.[39]

The sol-gel process involved in the formation of silica alcogel is one of a large class of kinetic aggregation processes that have been the subject of intense study in recent years.[40] Computer simulations have indicated that these processes tend to form clusters with highly ramified, statistically scale-invariant, *fractal* structures.[41] The fractal dimension D_f depends on the details of the aggregation process. At one extreme, diffusion-limited aggregation (DLA) models[42] give $D_f=2.51\pm0.06$,[43] while at another extreme, reaction-limited cluster-cluster aggregation (CCA) models[44] give $D_f=1.98\pm0.04$.[45] Ex-

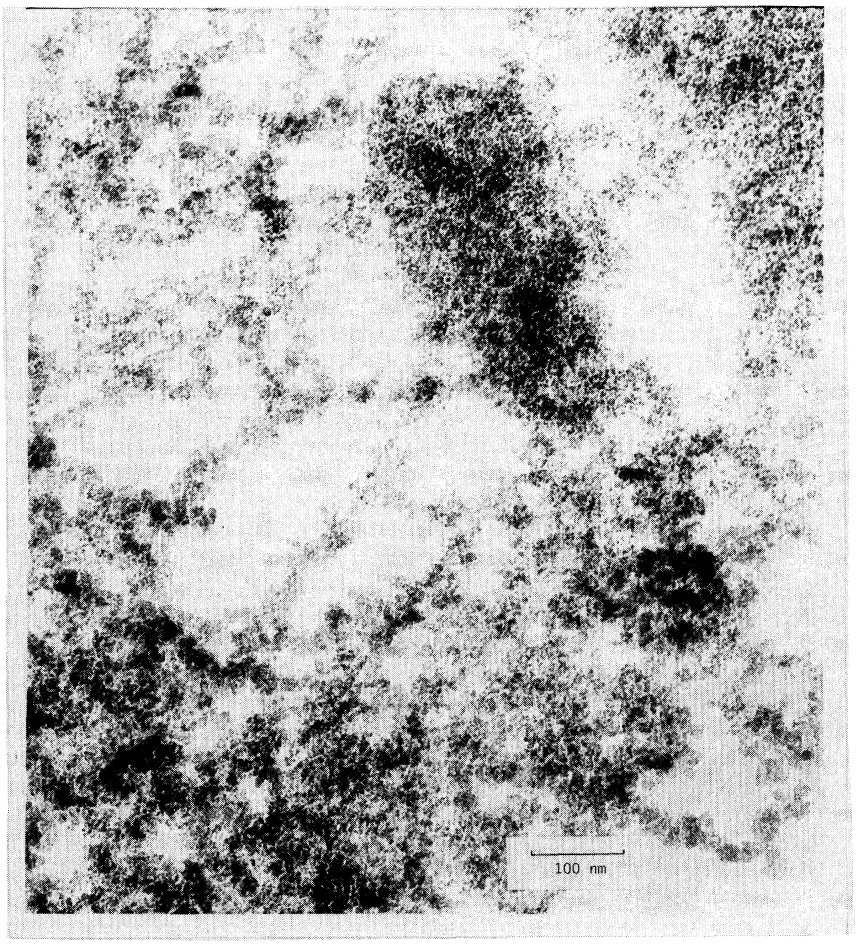

FIG. 3. This transmission electron micrograph of a carbon-coated flake of base-catalyzed aerogel was produced by Tewari, Hunt, Lieber, and Lofftus (Ref. 39). The pore space is shown in white and the scale bar at the bottom corresponds to a length of 100 nm.

perimental evidence for the existence of fractals in real aerogels has been somewhat qualified. Small-angle neutron scattering measurements by Vacher, Woignier, Pelous, and Courtens[22] on a series of *neutrally reacted* aerogels with densities from 0.095 to 0.356 g/cm^3 showed mutually self-similar fractal regimes spanning up to two decades in length, all with a fractal dimension of $D_f = 2.40 \pm 0.03$, and with the most extended power laws in the least dense samples. More recent light scattering data by Ferri, Frisken, and Cannell[46] on a variety of *undried* silica hydrogels, although mostly consistent with the data of Vacher *et al.*, indicated that the fractal dimensions could vary from 2.4 down to 2.1, depending on the gelation conditions, but nevertheless within the bounds imposed by the idealized models of DLA and CCA. Vacher *et al.* also found that the scattering intensities for their *base-catalyzed* aerogels could not be described by a single fractal exponent, in agreement with the previous x-ray scattering measurements by Schaefer and Keefer[23] on base-catalyzed aerogels obtained from Airglass. This is important because both of our aerogels were base-catalyzed.

C. Comparison with porous Vycor glass

For the purpose of this comparison, we need only point out that the pore structure in Vycor is noticeably more uniform than that in aerogel. This is immediately apparent in the transmission electron micrograph of Levitz, Ehret, Sinha, and Drake,[47] which is reproduced in Fig. 4. The underlying reason for this difference rests in the fundamentally different process that is used to make Vycor. Vycor is manufactured from a melt of borosilicate glass which is rapidly cooled below its demixing temperature, forcing it to *spinodally decompose* into a SiO_2-rich phase and a B_2O_3-rich phase. The latter phase is leached out with a suitable acid, leaving a porous SiO_2-rich glass that we call Vycor. In fact, this porous glass is just a precursor product in the production of a dense SiO_2-rich glass that Corning sells under the brand name Vycor. Unlike the aerogel structure, which is built up by a kinetic aggregation mechanism, the Vycor structure is formed all at once throughout the melt as it separates into little globules of SiO_2-rich and B_2O_3-rich phases. This is why the pore space tends to be much more uniform, with structure only on the length scale of the pores, as indicated by the peak in the neutron scattering data of Wiltzius, Bates, Dierker, and Wignall,[48] and in agreement with the theories of spinodal decomposition by Cahn.[49]

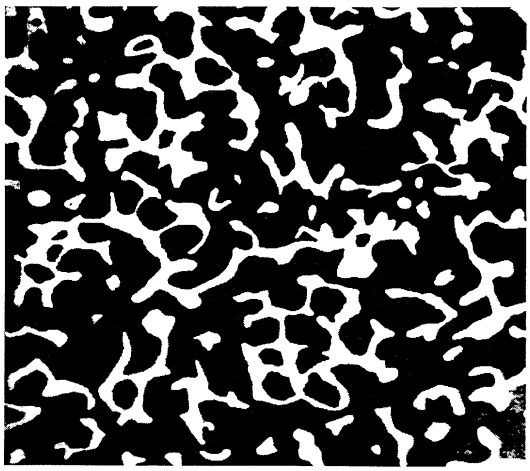

FIG. 4. This digitally enhanced transmission electron micrograph of a thin 35-nm slice of resin-filled Vycor was produced by Levitz, Ehret, Sinha, and Drake (Ref. 47). The pore space is shown in white and the horizontal scale is 800 nm.

III. OSCILLATORS

The principles of a torsional oscillator are outlined in a chapter from the low-temperature techniques book edited by Richardson and Smith.[50] This section will be limited to those details that are specific to the *low-frequency* oscillators that we have used to do our critical point measurements.

A. Low-frequency design and operation

All torsional oscillators are susceptible to sound resonance problems. For a cylindrical sample of radius r and height h, these resonances occur when the oscillator frequency f and the sound velocity c satisfy the relation[51]

$$f = \frac{c}{2}\left[\left[\frac{n_z}{h}\right]^2 + \left[\frac{\alpha_{mn}}{r}\right]^2\right]^{1/2}, \tag{22}$$

where $n_z = 0, 1, 2, 3, \ldots$ and α_{mn} are the roots of the Bessel function equation $[dJ_m(\pi\alpha)/d\alpha] = 0$. If $h = 2r$, as is usually the case in our cells, the sound modes appear in the order $mnz = 001, 100, 101, 200, 002, \ldots$ with $2hf/c = 1, 1.172, 1.541, 1.944, 2, \ldots$, respectively, as $c \to 0$. The characteristic length for coupling to an oscillator substrate is determined by the viscous penetration depth $\delta = \sqrt{2\eta/\rho\omega}$, where η is the normal fluid viscosity, ρ is the normal fluid density, and ω is the oscillator frequency. Near the λ point, δ is 5 μm at 200 Hz. Pore sizes are generally much less than δ, so in a conventional porous medium this would mean that only the superfluid is free to move and the relevant sound mode is fourth sound.[52] For a highly compressible porous medium like aerogel, however, the normal fluid can also move, in tandem with the glassy backbone, and the relevant excitation is the second-sound-like mode discussed by McKenna, Slawecki, and Maynard.[53]

The crucial observation is that there are an infinite number of temperatures at which this resonance condition is satisfied because, as $T \to T_c^-$, the sound velocity goes to zero. This is a problem because the best tracking circuits invariably use a phase-sensitive detection scheme to lock onto the oscillator. Sound resonances distort the oscillator phase and introduce S-shaped wiggles in the period output as a function of temperature. We never did get rid of this problem, strictly speaking, but we were able to make the oscillator frequency so low and the sample cell so small that the sound resonances occurred too close to T_c to affect our critical point measurements. In particular, we chose to operate our aerogel oscillators in the 150–300 Hz range. Although our BeCu torsion rods were only 0.53 mm in diameter, they were still not thin

enough to achieve the desired frequencies. The sample cell holders had to be made more massive to compensate, but because our oscillators had a very high signal-to-noise ratio to begin with, the resultant loss in sensitivity was not important. Typical sample cell sizes were about 6 or 7 mm in both diameter and height. More precise dimensions are given in Table I. The overall cell layout is depicted in Fig. 5.

The oscillators were usually driven by one of our homemade "torsional oscillator automatic drive systems" (TOADS boxes). A block diagram of this circuit is depicted in Fig. 6. Occasionally, we also used a PAR 124 lock-in amplifier in the feedback circuit devised by Agnolet, McQueeney, and Reppy.[54] All of our BeCu oscillators were nonlinear,[55] meaning that the resonant frequencies were a weak function of the oscillator amplitude. Typical values of $(\delta f/f)/(\delta A/A)$ were 4×10^{-5}. Since the total cell dissipation changed by about a factor of 1.4 as we swept through the transition, we tried to operate our oscillators in a constant amplitude mode, whenever possible, by using our data acquisition system to adjust the drive level every 15 sec. As it turned out, the critical exponents were quite resilient to changes in the operating condition. For example, with sample E in the simultaneous ρ_s and C measurement, we used the TOADS box in a constant amplitude configuration. Afterwards, we warmed up, removed the thermal isolation superleak, and repeated the ρ_s measurement using the PAR 124 lock-in in a constant drive configuration. The empty cell oscillator was about four times more lossy the second time around, due to a bit of silver paint that we accidentally deposited on the torsion rod, but the filled cell period stability was not affected. Even more important, no discernible change in the superfluid density exponent was observed. We summarize our drive conditions in Table II.

Capacitive electrodes, biased at 180 V dc, were used both to drive and to detect the oscillator motion. These electrodes have a known side effect.[50] They change the torsional spring constant by

$$\Delta K = -CV_0^2\left[\frac{r}{d}\right]^2, \tag{23}$$

where C is the electrode capacitance, V_0 is the dc bias voltage, r is the radial distance from the electrode to the torsion rod, and d is the capacitor gap. Notice that the sign of this spring constant effect does not depend on the electrode orientation. This effect is particularly severe in a low-frequency oscillator because the torsion rod is very compliant. Our torsion rods had spring constants of 7.2×10^{-2} N m, versus a total contribution of 8.1×10^{-5} N m from the two-electrode drive and detect system. In order to get a period stability of better than 1 part in 10^8, the drift in the dc bias voltage has to be less than 10 ppm. Conventional batteries are not this stable and so we regulated our bias voltage by using a simple op-amp circuit to add a correction voltage to the battery output. Over a three to four day test period, we found that our 180 V dc regulated batteries were stable to within the ±1 mV resolution of our voltmeter.

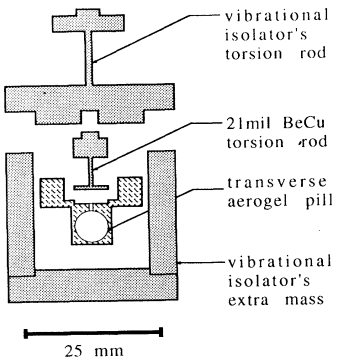

FIG. 5. This is an exploded cross-sectional view of our low-frequency torsional oscillator. The sample head was made of aluminum, but the torsion rod and vibration isolator were made of BeCu. The vibration isolator structure was also designed to serve as a protector for the delicate torsion rod. Two "ears" on the sample head formed one-half of our capacitive drive and detect system. Complementary electrodes (not depicted here) were attached to the vibration isolator structure.

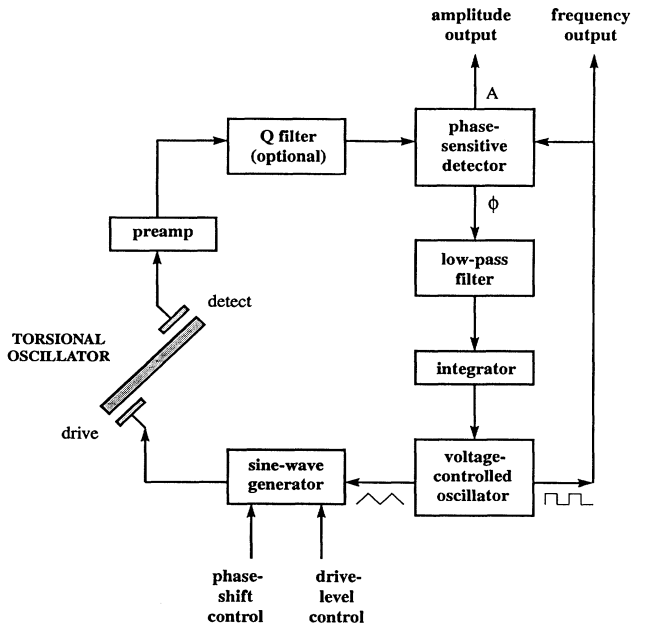

FIG. 6. This is a block diagram of one of our torsional oscillator automatic drive systems or TOADS boxes. The feedback circuit formed by the phase-sensitive detector, low-pass filter, integrator, and voltage-controlled oscillator is a phase-locked loop that tracks the frequency of the torsional oscillator. It is used as a part of the larger feedback circuit that drives the torsional oscillator. The phase of the sine-wave generator must be adjusted to compensate for the shifts due to the torsional oscillator, the capacitive electrodes (whose dc bias circuitry is not depicted here), and the preamp. A third feedback loop, implemented in software by our data acquisition system, adjusts the magnitude of the drive signal in order to maintain a constant amplitude for the oscillator motion.

TABLE II. The oscillator parameters listed here are the frequency and amplitude at the superfluid transition, and the hydrodynamic χ factors at the gross, macroscopic, and microscopic levels.

Sample	ρ (g/cm^3)	f (Hz)	A (10^{-6} rad)	χ	χ_M	χ_m
A	0.133	153.5	51	not available	not available	not available
B	0.133	203.8	76	0.334	0.207	0.161
E	0.133	141.9	238	0.329	0.212	0.149
F	0.200	293.8	543	0.163	0.0	0.163

B. Large-scale hydrodynamic corrections

Ideally, the superfluid mass is decoupled from the torsional oscillator because its viscosity is identically zero. In any real porous medium, however, the flow path is always tortuous and even a zero viscosity superfluid will impart some resistance, called *inertial drag,* to the motion of the porous substrate. Following Mehl and Zimmerman,[56] we have defined the χ factor as the fraction of the superfluid mass that is effectively coupled to the porous substrate. χ is zero in the ideal case. A deeper understanding of these effects is important because, ultimately, they determine the magnitude of the heat-capacity singularity.

For incompressible superfluid flow, we can write the velocity as the vector gradient of a scalar potential ϕ, namely, $\mathbf{v}_s=\nabla\phi$. If the oscillator is rotating at a constant angular velocity ω, then linearity implies that we can write the scalar potential as $\phi(\mathbf{r})=\omega B(\mathbf{r})$, where $B(\mathbf{r})$ is some function of the porous structure. Since the flow is inviscid, velocity transients cannot decay with time and, therefore, there can be no such transients. The flow field must respond instantaneously to any change in $\omega(t)$, meaning that we can write

$$\phi(\mathbf{r},t)=\omega(t)B(\mathbf{r})\ . \tag{24}$$

This result makes it easy for us to calculate the effective moment of inertia from the ratio of the time derivative of the angular momentum to the angular acceleration. The χ factor is then defined as the ratio of this effective moment of inertia to the solid body moment of inertia of the helium inside the porous medium:

$$\chi\int[r_\perp^2 C(\mathbf{r})]d^3r=\int[\mathbf{r}\times\nabla B(\mathbf{r})]d^3r\ , \tag{25}$$

where $C(\mathbf{r})$ is defined to be 1 when $\mathbf{r}$ is in the pore space and 0 when $\mathbf{r}$ is in the glass. Notice that by defining χ in these terms, we have averaged out any small-scale inhomogeneities in the porous structure.

Superfluid mass in ^{4}He-filled porous media can be measured by torsional oscillator or fourth-sound experiments. These two techniques are complementary, and this is reflected in a relation between the χ factor and the acoustic index of refraction n. The underlying reason for this relation's existence is that both problems require a solution of Laplace's equation with the same boundary conditions. However, the relation can be more easily derived through an energy argument. Suppose we rotate the sample at ω, cool through the superfluid transition, and then stop rotating the sample. A persistent current will be set up. How should we account for the tortuosity of the porous medium in our expression for the kinetic energy of the superfluid? We can put a correction factor into our definition of either the moment of inertia or the angular velocity. In the first case, the effective moment of inertia is $(1-\chi)I$, where I is the solid body moment of inertia of the helium inside the porous medium. Alternatively, since waves propagating through a refractive medium transport energy at the group velocity, we can replace ω with (ω/n). Equating these two equivalent expressions for the kinetic energy, we find that

$$n^2=(1-\chi)^{-1}\ , \tag{26}$$

in agreement with the more detailed calculations of Yanof and Reppy, as well as Bergman, Halperin, and Hohenberg.[57]

Interpretations for samples B and E were further complicated by the fact that the axis of the aerogel cylinder was oriented perpendicular to the torsion rod. We did this to improve the oscillator stability because we found that, in a conventional colinear configuration, *unglued* aerogel cylinders grasped by their circumference would slip. Flipping the cylinder over by 90° ensured that it would be pushed back and forth instead. The transverse orientation introduced a χ factor of its own, which we had to compute numerically, starting with Fetter's[58] solution for the χ factor of a rectangle with sides a and b, rotation axis perpendicular to and centered on the rectangle. This $\chi_r(b/a)$ was written in the form of a rapidly convergent series, for which the first three terms inside the summation ensured at least six digits of accuracy:

$$\chi_r\left[\frac{b}{a}\right]=\frac{1}{1+(b/a)^2}\left[1-3\left[\frac{b}{a}\right]^2+\frac{744\zeta(5)}{\pi^5}\left[\frac{b}{a}\right]^3-\frac{1536}{\pi^5}\left[\frac{b}{a}\right]^3\sum_{n=0}^{\infty}\frac{1}{(2n+1)^5\{\exp[(2n+1)\pi a/b]+1\}}\right]\ . \tag{27}$$

The symmetry relation $\chi_r(b/a)=\chi_r(a/b)$ was used to ensure that b/a was always a small number in the series expansion. After a suitable integration, we got $\chi_c(d/h)$, the χ factor for a cylinder of diameter d and height h, rotation axis perpendicular to the cylinder axis and centered along its length. The idea was to add up the moments of inertia for infinitesimal rectangular slabs, each weighted by χ_r, and then normalize by the moment of in-

ertia for the entire cylinder, giving

$$\chi_c\left[\frac{d}{h}\right]=\frac{2\int_0^{(d/2h)}\{\frac{1}{12}b(z)[1+b(z)^2]\}\chi_r(b(z))dz}{\pi(d/2h)^2\{\frac{1}{12}+\frac{1}{4}(d/2h)^2\}}\ , \tag{28}$$

where $b(z)=2\sqrt{(d/2h)^2-z^2}$. Notice that χ_r and χ_c depend only on the aspect ratios b/a and d/h. They are invariant against isotropic changes of scale because, in a zero viscosity fluid, there is no characteristic length.

The gross χ factor was obtained from a combination of oscillator periods for the empty and filled cell, denoted as P_e and P_f. A simple three-step procedure was used to compute, in order, the background-corrected period ΔP, the superfluid period shift ΔP_s, and the gross χ factor:

$$\Delta P(T)=P_f(T)-P_e(T)\ , \tag{29}$$

$$\Delta P_s(T)=\Delta P(T_\lambda)-\Delta P(T)\ , \tag{30}$$

$$(1-\chi)=\Delta P_s(0)/\Delta P(T_\lambda)\ . \tag{31}$$

The gross χ factor was subsequently decomposed into a macroscopic term χ_M due to the transverse mounted cylinder, and a microscopic term χ_m due to the tortuosity of the porous medium:

$$(1-\chi)=(1-\chi_M)(1-\chi_m)\ . \tag{32}$$

There is no way to decouple the evaluation of a χ factor from the assumption of a unity value for the zero-temperature superfluid fraction, short of explicitly calculating the χ factor itself. In the case of ^{3}He dissolved in ^{4}He, the superfluid fraction is definitely not unity at zero temperature.[59] Since our assumption breaks down in the annealed impurity case, we can think of no compelling reason why it should hold in the quenched impurity case. However, in analogy with the microscopic theory of Feynman,[60] which treats the motion of a ^{3}He atom through the ^{4}He background as a microscopic hydrodynamic problem not unlike a χ factor calculation, one might argue that χ factors are just another way to express the same physics that might otherwise be represented by a nonunity value of the zero-temperature superfluid fraction. We shall assume this to be so without further argument and summarize our calculations in Table II.

In the final section, we will argue that the fluctuation contribution to the heat-capacity singularity is governed by a quantity that we call the *coarse-grain averaged* superfluid density $\tilde{\rho}_s$, which is the superfluid density averaged over the entire sample volume. For now, we merely define it in terms of the measured numbers. We start with the oscillator's mass sensitivity dm/dP, given by

$$(1-\chi_M)\frac{dm}{dP}=\frac{\rho V}{\Delta P(T_\lambda)}\ , \tag{33}$$

where ρ is the density of liquid helium and V is the open pore volume in the sample cell. The coarse-grain averaged superfluid mass is defined as $\tilde{m}_s=(dm/dP)\Delta P_s$. The coarse-grain average volume is taken to be $\tilde{V}=V/\mathcal{P}$, where $\mathcal{P}$ is the porosity of the aerogel. This might seem unusual at first, but it is not, because, in the impurity interpretation that we have adopted, the sample volume must include both the helium and the aerogel. These definitions can be reduced to one simple equation:

$$\tilde{\rho}_s(T)=[(1-\chi_m)\mathcal{P}]\rho_s(T)\ . \tag{34}$$

Everything conspires to make $\tilde{\rho}_s$ smaller than ρ_s. Packed powder experiments[52] indicate that χ factors tend to increase when the porosities decrease. So, highly porous media such as aerogel tend to have $\tilde{\rho}_s$ that are not much different in magnitude from bulk helium, whereas less porous media such as Vycor have $\tilde{\rho}_s$ that are significantly smaller.

IV. CALORIMETRY

In adiabatic calorimetry, the quality of the thermal isolation is at least as important as the quality of the thermometry. Thermal isolation is a particularly difficult problem when there is superfluid helium inside the fill line. For our low-resolution experiments, samples C and E, we packed 10–80 nm jeweler's rouge into the fill line in order to make a superleak plug through which normal fluid counterflow was forbidden, and hence through which no superfluid heat transport would occur. The thermal isolation provided by the superleak plug was not ideal,[61] so resistance thermometry sufficed for these runs. For samples D and G, a low-temperature valve was used instead. This solved our thermal isolation problem, and it made worthwhile the installation of a high-resolution superconducting quantum interference device (SQUID)-based magnetic thermometer. The resultant setup was able to measure heat capacity to 100 ppm using temperature steps of only 30 μK, and it is the subject of the remainder of this section.

A. SQUID-based magnetic thermometer

The high-resolution magnetic thermometer that we used was originally developed by Lipa and co-workers.[62] The temperature-dependent quantity measured was the magnetization of a sample of copper ammonium bromide (CAB) salt, $Cu(NH_4)_2Br_4\cdot 2H_2O$, that was subjected to the extremely stable magnetic field inside a superconducting niobium tube. CAB is a 3D Heisenberg ferromagnetic insulator[63] with an ordering temperature of 1.8 K. The salt crystals were mounted inside a $\frac{1}{8}$ inch length of a 4-40 tapped hole, using an Allen head screw to crush and compress them into this 0.016-cm^3 sample volume. Threaded walls improve thermal contact by doubling the surface area shared by the salt and the copper cell body. Judging from our raw $T(t)$ data, the thermal relaxation time between the sample and thermometer was around 30 sec.

Figure 7 depicts the complete magnetometer system. Temperature-induced *changes* in the magnetization of the CAB salt were coupled to a rf SQUID by a superconducting dc flux transformer. All of the important SQUID electronics, as well as the SQUID itself, was purchased from BTI.[64] The homemade rf probe was a more or less exact imitation of BTI's triax and tuning circuit, adjusted to accommodate our special spatial constraints. Al-

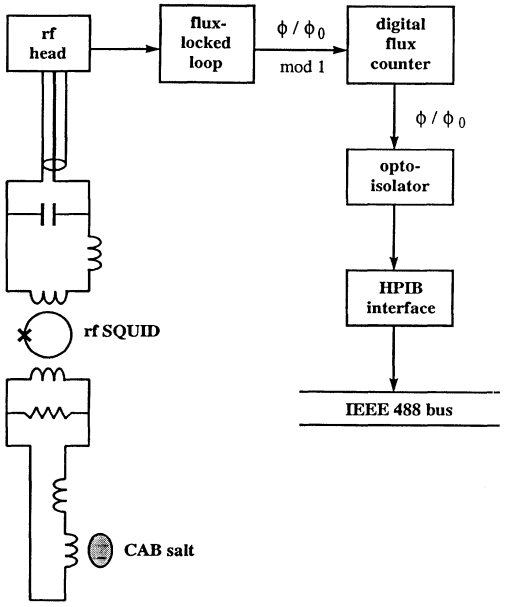

FIG. 7. This is a block diagram for our SQUID magnetometer. It was not possible to fully shield the superconducting dc flux transformer from rf noise, so a 2.7-Ω shunt resistor was placed across the 2-μH input coil to create a low-pass filter. The LC tuning network at the bottom of the triax was adjusted by trial and error to suit the 19-MHz circuitry on the rf head. All of the SQUID circuitry (the Model-300 rf head, the Model-30 flux-locked loop, and the Model-DFC digital flux counter) was purchased from BTI.

though the flux-locked loop (FLL) was extremely sensitive to small changes in the magnetization, its analog output was inherently incapable of the dynamic range that we needed. This problem was solved by limiting the FLL output to $\pm 1\phi_0$ and than counting ϕ_0's to compensate, using the digital flux counter (DFC). The flux counter output was a nine-digit number for which the first five digits represented the ϕ_0 count and the last four digits represented the fractional ϕ_0 signal coming out of the FLL circuit. When the FLL was set to its slow mode, with a 10-Hz output filter, we got a rms flux resolution of $2\times 10^{-3}\phi_0$ at a maximum slew rate of about 500 ϕ_0/sec.

Since we had to maintain a continuous record of the flux count, we were constantly on the lookout for anything that might disturb our flux counting system. We found that routine transfers of liquid helium into the bath would sometimes upset the flux count by tens of ϕ_0. The flux jumps occurred when the transfer stick was first inserted into the Dewar. The telltale signature was a sharp lurch in the $\phi(t)$ chart trace that was not accompanied by a corresponding change in the cell's resistance thermometer. To be safe, we always backed up after a transfer and retook a few of the data points that were measured just before the transfer. Later on, we examined the overlapping heat-capacity data from before and after the transfer to determine if a flux jump occurred and, if so, how much. We then shifted our $T(\phi)$ calibration by some integral number of ϕ_0's in order to get the data to merge. In most cases, this allowed us to correct the flux jump down to the final ϕ_0. At the end of the run on sample D, in order to see how well we kept track of things, we backed up and retook seven additional heat-capacity data points, evenly spaced over the critical region, with no intervening transfer. All of these retakes came within 30–70 ppm of the original data.

The temperature dependence of the magnetization was a function of the size of the trapped field. At temperatures well above the CAB ordering transition, we found that the magnetization scaled more or less linearly with the applied field, in accordance with expectations based on assumptions of a simple Curie-Weiss susceptibility. Nearer the ordering transition, and in accordance with expectations based on theories of critical phenomena, larger applied fields smeared out the magnetization signal. The ordering transition also contributed a small singularity to the heat-capacity background. Just as with the magnetization signal, this singularity was smeared out as the applied field was increased. All of these field dependencies are depicted in Fig. 8. $\phi(T)$ was calibrated against a carbon glass resistor that was mounted on the cell. Absolute accuracy was about $\frac{1}{2}$ mK, which was sufficient because critical exponents are, to first order, invariant against smooth distortions of the temperature scale. Critical exponents are also insensitive to small drifts in the thermometry, so we did only a simple test to verify that the λ point, as determined through repeated heat-capacity measurements, was stable to at least a μK over a day or two.

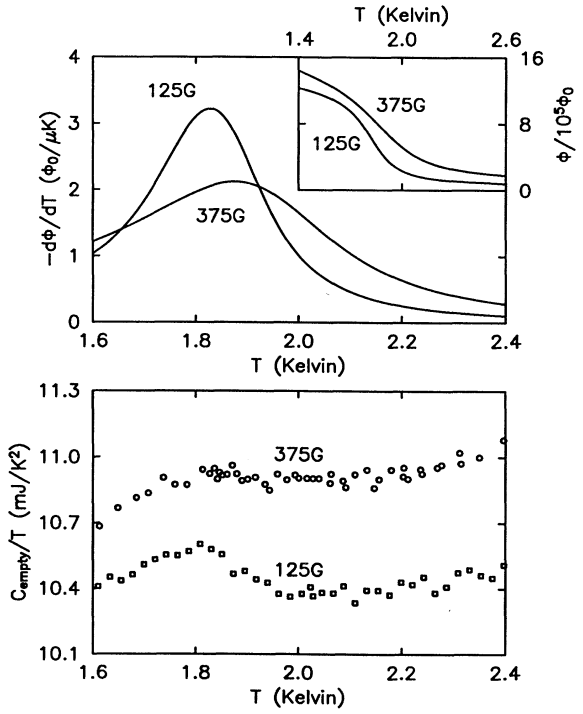

FIG. 8. Increasing the applied field smears out the CAB ordering transition. This effect is seen in both the magnetization ϕ and the heat-capacity background C_{empty}. The vertical shift in the two heat capacities is a result of our having switched to a more massive valve assembly between runs.

We usually trapped a field of 375 G inside our niobium tube, which gave us a sensitivity of 0.74 ϕ_0/μK near T_λ. This resulted in a rms temperature resolution of just under 3 nK, from 2.2 K down to at least 1.4 K. The thermal fluctuation limit is $\delta T/T=(2k_B/C_M)^{1/2}$, which worked out to 0.8 nK for our quantity of CAB salt.

B. High-resolution heat capacity

Figure 9 depicts the complete high-resolution aerogel heat-capacity cell. In spite of the fact that there was a lot more metal than helium in this design, the heat capacity due to the helium inside the aerogel, near the superfluid transition, was 50 times larger than the background heat capacity. The capacitive liquid level sensor above the aerogel was used to verify that we always had a liquid-vapor interface, even as the volume of the liquid inside the cell changed with temperature, ensuring that our experiment always operated at saturated vapor pressure.

Spatial constraints dictated that we had to use a hydraulic mechanism to actuate the valve, as opposed to a mechanical one. Since we were using ^{4}He as our hydraulic fluid, we had to design the valve so that the actuator line could be pumped out without undoing the seal, or else the helium inside the actuator line would have given us a thermal short. Our idea was to make an indium O-ring joint *in situ,* at low temperatures, and with such high actuator forces that the indium would cold weld. After numerous failures, we decided that since it was the surface normal force that caused the indium to flow and make a seal, *blunt* stems would work better. Our most reliable valves used a 60° stem and a 120° seat. Both pieces were machined from brass and then coated with a thick 0.1–0.3 mm layer of indium. The stem was mechanically coupled, but not physically attached, to the bellows actuator. Thus it would be pushed into the seat when the bellows were pressurized, but it would not be pulled back out when the bellows were evacuated. Since the indium joint was not very strong, the stem popped off benignly when the cell was warmed up at the end of the run. With our $\frac{5}{8}$-in.-diam bellows, we found that at least 400 psi of pressure, equivalent to an actuator force of 120 lb, was needed to make the valve seal. We never tried to reuse any of our stems or seats because they were both visibly deformed after just one operation.

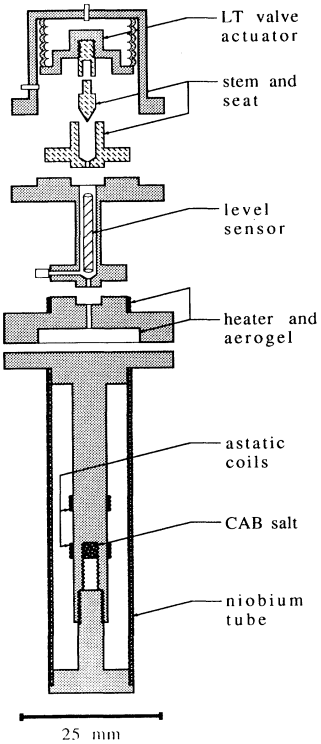

FIG. 9. This is an exploded cross-sectional view of our high-resolution heat-capacity cell, which was suspended from the stage by three hollow Vespel rods and then enclosed by a radiation shield that was thermally anchored to the stage. The valve assembly was made of unannealed BeCu, but everything else was made of oxygen-free high-conductivity (OFHC) copper.

Once the valve was pumped out, we were left with a cell that had a very large heat capacity and was extremely well isolated from the rest of the cryostat. For sample D, the thermal isolation time between the stage and the cell was 3.0 *days* near the heat-capacity maximum at the superfluid transition, which corresponded to a thermal conduction of 4.3 μW/K between the stage and the cell. This was the same thermal conduction that we measured before the cell was filled, and we interpreted this agreement as proof that our valve was working. For most of the first week after an initial cool down, there was a slow time-dependent heat leak into the cell. We suspect that this was due to the aerogel glass and/or our various epoxy joints. Glassy materials like these are known to be a source of such time-dependent heat leaks.[65] Since this virtual heat leak could be tens of nW, we were not able to take reliable data until it decayed away. Therefore our slow startup procedures (three to four days to pump out the valve, another two to cool the cell down) were not a hindrance.

Current flowing through the 407-Ω noninductive cell heater was monitored using a stable (4 ppm/K) room-temperature series resistor. Our data acquisition system maintained its own estimate of the most recently measured heat capacity in order to compute just how much energy was needed to either step to the next data point or to take a heat-capacity measurement. In the latter case, the heater powers were usually chosen to make the pulse width 1 min long. Somewhat longer pulses, up to 5 min, were used for the biggest temperature steps when our heater output saturated. Typical heater powers ranged from 35 nW, when taking 2-μK steps near T_λ, up to 8 μW, when taking 1-mK steps far below T_c. The temperature steps were chosen to be no bigger than the distance to the next data point, and always less than 1 mK, to ensure that the critical point singularity would not be smeared out.

Each pulse measurement generated a separate file containing a curve of temperature versus time (sampled every 10 sec), a curve of heater current versus time (sampled every 2 sec, filed only during the pulse), and a few other associated numbers such as the pulse width and the pulse location. A sample pulse and fit deviation is shown

in Fig. 10. Our fitting function, $T(t)$, varied with the size of the temperature step. In most cases, for step sizes between 20 and 200 μK, we fitted to a common linear background drift on both sides of the pulse, plus an exponential decay contribution after the pulse. Assuming that the heater pulse started at t_1 and ended at t_2, we fitted to

$$T(t)=T_0+\delta T_1 t+\{T_2\exp[-(t-t_2)/\tau] \text{ for } t>t_2\} . \tag{35}$$

The fit was restricted to data with $t<t_1$ or $t>t_2+t_{\text{smear}}$, where $t_{\text{smear}}=180$ sec was needed because the temperature decay would not achieve steady state until some time after the heater was shut off. We could have fitted to an exponential decay on both sides of the pulse, with a fixed baseline defined by the stage temperature, but δT_1 was usually too small, less than 0.1 nK/sec, to justify this extra complication. To compensate for the heater power lost through conduction across the weak thermal link between the stage and the cell, it sufficed to evaluate the temperature rise at the midpoint between t_1 and t_2. This approximation is correct insofar as the temperature rise during the heater pulse is linear in time, or equivalently, if the rate of heat conduction between the stage and the cell is small compared to the heater power. For the smallest step sizes, our nonlinear least-squares algorithm often crashed with $\tau=0$ or ∞. So we simply fitted $T(t)$ with two straight lines. At the other extreme, for the largest step sizes, Eq. (35) was not able to fit the data above t_2 because τ was temperature dependent. To avoid the obvious recursion problem, we took advantage of the fact that τ was huge on the time scale of our pulse measurement. Hence the exponential decay in $T(t)$ was linear to the first two digits and we could approximate τ as a weakly linear function of time. This took care of the fit deviations that would have otherwise appeared on the fifth digit of the temperature rise.

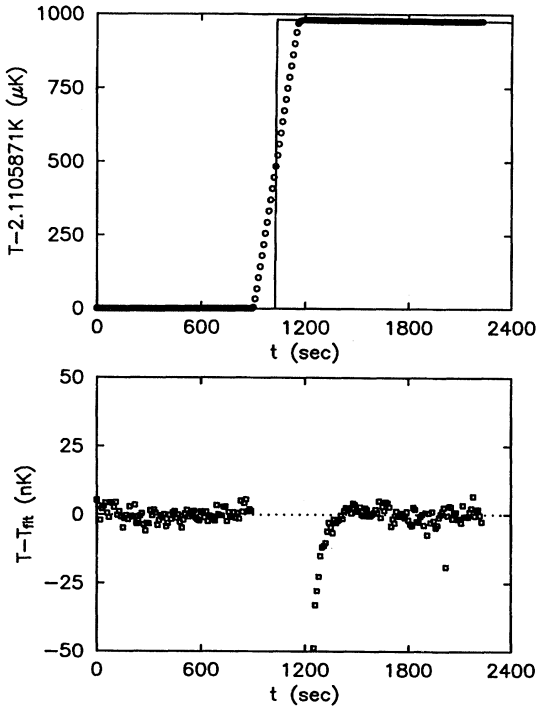

FIG. 10. This is a 1-mK pulse measurement from the sample-D run. Bad points like the one seen near 2000 sec occasionally appear during a flux count and reset operation when the $\frac{1}{6}$-Hz sampling circuit in the DFC happens to catch the low-pass filtered FLL output in midflight. They are easily ignored by our fit routines.

V. RESULTS

The most direct criterion for a *dilute* impurity is that the depression in the transition temperature that it induces must be small compared to the pure system T_c. Table I confirms that aerogels satisfy this criterion because the observed shifts are not more than 4×10^{-3} of the pure system T_c. Although aerogels have only a tiny effect on the transition temperature, we shall see that they have a very dramatic effect on the critical exponents.

A. Superfluid density power-law behavior

Figure 11 depicts the superfluid density, normalized to one at zero temperature, for our two representative aerogels. The difference in curvature between these data and the bulk helium line demonstrates that these data are not bulklike. Detailed magnifications shown in Figs. 12 and 13 indicate that even our worst samples had transitions that were sharp to at least 10^{-4} in reduced temperature. Starting at about 200 μK below T_c, and ending more or less at T_c, there was a pronounced dip in the dissipation data. In samples E and F, there were also an accompanying kink in the oscillator period. We doubt that this feature was due to a sound resonance problem because our estimates indicate that such resonances should not have occurred this far out from T_c. Furthermore, sound resonances usually lead to a series of sharp wiggles in the dissipation, not one steady drop. A single steady drop is consistent with a critical velocity effect, but we did not test this hypothesis out.

A number of unexpected effects were seen *above* the

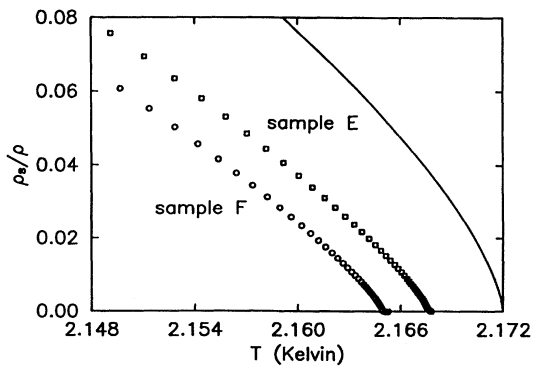

FIG. 11. Normalized superfluid density data for sample E (0.133 g/cm^3 DESY aerogel) and sample F (0.200 g/cm^3 Airglass aerogel) are plotted alongside a solid line representing the superfluid fraction in bulk helium (Ref. 13).

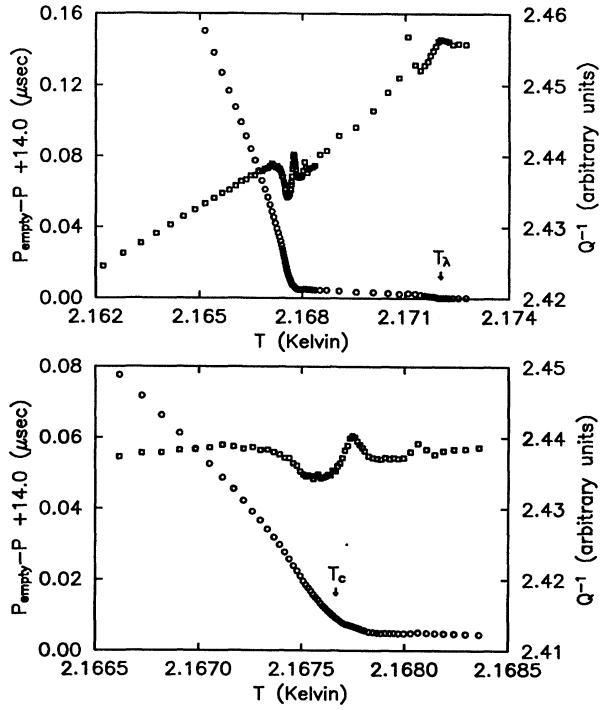

FIG. 12. The oscillator period shift (○) and dissipation (□) for sample E are plotted on a linear scale to emphasize the variety of things that can happen near T_c, as well as between T_c and T_λ. The wiggles in the dissipation between T_c and T_λ are due to sound resonances in the percolating network of large voids.

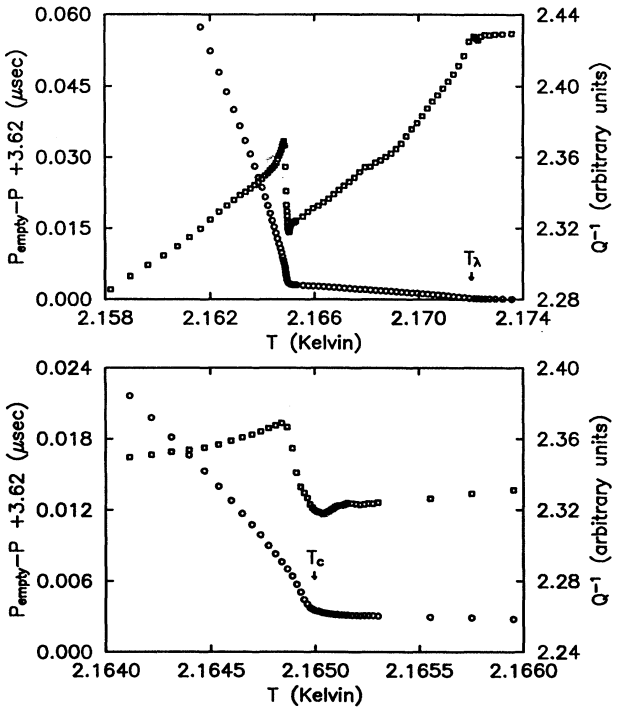

FIG. 13. The oscillator period shift (○) and dissipation (□) for sample F are plotted on a linear scale to emphasize the variety of things that can happen near T_c, as well as between T_c and T_λ. Notice how the bottom of the dissipation drop seems to coincide with T_c, in this figure as well as Fig. 12.

aerogel transition. We found that the dissipation continued to increase after T_c, and did not stop until T_λ. There was also a residual amount of superfluid mass decoupling between T_c and T_λ, as if there were large voids within the aerogel itself, some fraction of which must have formed a percolating network because isolated pockets of superfluid cannot decouple from an oscillator. This is admittedly a simplistic interpretation because both transitions, aerogel and bulk, occur within the same body of liquid helium. We are essentially assuming that there is a big gap in the pore size distribution, between those pores responsible for the aerogel transition and the voids that we have postulated. Recent experiments by Ma and Chan[66] support our hypothesis that this residual mass decoupling is an artifact because no such feature is seen when the aerogel is grown *in situ*. Although the singularity in the void signal was located far enough from T_c that it did not affect our power-law fits, we nevertheless subtracted it off. The void contribution was determined by a fit to just the end points at T_c and T_λ because the oscillator signal in the intermediate region was too highly distorted by sound resonances to allow a full curve fit. These fit results are listed in Table III. Extrapolated back to zero temperature, the void signal was typically 2% of the total superfluid signal.

The most important adjustable parameter in a power-law fit is the transition temperature T_c. We used two different algorithms to pick the optimal T_c. In both cases, we started by declaring a range of reduced temperatures for the power-law fit, and then selecting out for further analysis only those points that fell within this range. In our first algorithm, we used a brute force non-

TABLE III. The background-corrected period at T_λ was used as a baseline from which the superfluid period shifts were computed. The void contribution was fitted using just the end points at T_c and T_λ, then subtracted off. The remaining period shift was attributed to the aerogel transition at T_c. For comparison, both superfluid components have been extrapolated back to zero temperature.

Sample	ρ (g/cm^3)	$\Delta P(T_\lambda)$ (μsec)	$\Delta P_{s,\text{aerogel}}(0)$ (μsec)	$\Delta P_{s,\text{voids}}(0)$ (μsec)
A	0.133	not available	6.5410	0.2140
B	0.133	9.5519	6.3573	0.1618
E	0.133	13.9498	9.3548	0.1283
F	0.200	3.6182	3.0281	0.0576

linear least-squares (NLS) fit on the functional form

$$\rho_s(T)=\rho_{s_0}(1-T/T_c)^{\zeta}+\rho_c \ , \tag{36}$$

where ρ_c compensated for the slight error, less than 1 part in 10^4, in the superfluid density baseline that we established by eye. The weight function $w(T)$ must be set to the inverse square of the expected deviations and/or noise. Based on an analogy with the bulk helium fits,[13] we assumed that higher-order corrections to scaling would take the form $|t|^{\zeta}(1+b|t|^{\theta})$, with the confluent exponent $\theta=0.5$. So our weight function became

$$w(T)=[(1-T/T_c)^{2(\zeta+0.5)}+w_0]^{-1} \ , \tag{37}$$

where w_0 was used to account for the noise in the data closest to T_c. If this noise first became visible at a reduced temperature of t_0, where visible was taken to mean about 1% scatter, then we set $w_0=t_0^{2(\zeta+0.5)}$.

The NLS fit algorithm gave an overly optimistic estimate for the exponent uncertainty, and we preferred instead the numbers given by our second algorithm. First, the ρ_c determined by the NLS fit was accepted without question. Then a series of power-law fits was performed over a range of T_c. For each trial T_c, we derived a power-law fit from a linear regression on the log-log transformed ρ_s versus t data. The rms fractional deviation from each such power-law fit was then computed and plotted as a function of the resultant exponent ζ, as shown in Fig. 14. The *raw exponent uncertainty* was defined as the half-width at which these fit deviations were twice their minimum. This number was still too optimistic, as it did not account for changes in the exponent due to changes in the declared range of the power-law fit. The uncertainties listed in Table IV should probably be multiplied by $\sqrt{2}$ to take this into account. The optimal exponent derived from this algorithm always fell well within one error bar of the exponent derived from the original NLS fit. Incidentally, we did try this algorithm using absolute rather than fractional fit deviations, but we found that the resultant exponents were five times more sensitive to changes in the pre-selected range of the power-law fit.

Our first detailed superfluid density power-law fits were obtained for sample B. The saturated vapor pressure measurement is shown in Fig. 15. After taking these data, we pressurized the cell to 353 torr and made another measurement. Because the cell pressure was only passively regulated, using a 300-cm^3 room-temperature ballast volume, these data had a lot more scatter than usual.

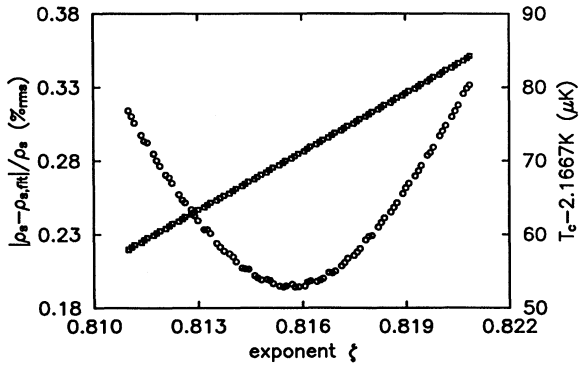

FIG. 14. For example B, the rms fractional fit deviations (○) are plotted as a function of the resultant exponent ζ. The raw exponent uncertainty is defined as the half-width at which the fit deviations are twice their minimum value. For comparison, the trial T_c (□) are also plotted.

Both transition temperatures, T_c and T_λ, were shifted by −3.90 mK, giving a slope of −119 atm/K for the λ line in ^{4}He-filled aerogel. For comparison, the bulk λ line has a slope of −118.4 atm/K. As expected from universality arguments, the critical exponent was not significantly altered.

The simultaneous ρ_s and C measurement was done on sample E. Since we were also set up to do a superfluid density exponent measurement, we did so, twice. The first run was done with the superleak isolator in place. The second was done after we warmed up, removed the superleak isolator, and then cooled down again. The ρ_s data listed in our tables for sample E come from this second run. No observable change in the critical exponent occurred as a result of thermal cycling, which means that aerogel is not significantly damaged by the surface tension of liquid ^{4}He.

The ρ_s data for sample F are representative of the newer aerogels that we purchased directly from Airglass. Figure 16 shows that these data had a slight 0.4% systematic deviation from perfect power-law behavior. Because there was also an unusual undulation in the dissipation data over the same temperature range, we do not know if this tiny deviation was an experimental artifact. Notwithstanding this very small deviation, this critical exponent is essentially identical to the one seen in the DESY aerogels. It is interesting that two aerogel samples with such different porosities can give the same ρ_s ex-

TABLE IV. From our power-law analysis of the superfluid densities, we have derived for each sample the critical temperature, the *coarse-grain averaged* critical amplitude, the critical exponent (plus or minus the raw exponent uncertainty), and the correlation lengths and reduced temperatures spanned over the power-law regime.

Sample	ρ (g/cm^3)	T_c (K)	$\tilde{\rho}_{s_0}$ (g/cm^3)	Exponent ζ	ξ range (nm)	t range ($\log_{10}$)
A	0.133	2.166 344	not available	0.820±0.127	not available	below −2.0
B	0.133	2.166 773	0.418	0.817±0.006	12.4 to 304	−3.7 to −2.0
E	0.133	2.167 663	0.403	0.802±0.005	12.0 to 334	−3.8 to −2.0
F	0.200	2.164 991	0.374	0.811±0.004	7.70 to 989	−4.3 to −1.7

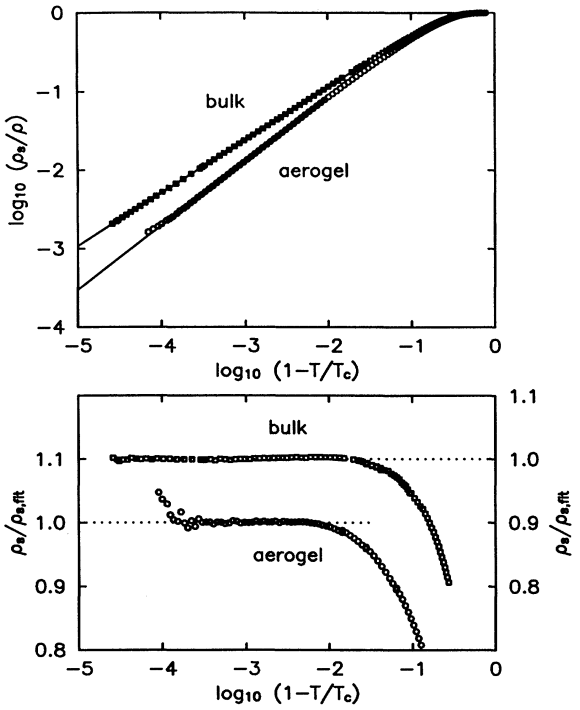

FIG. 15. This is the superfluid density power law for sample B, at saturated vapor pressure. For comparison, our aerogel data (○) are plotted alongside the bulk data (□) of Greywall and Ahlers (Ref. 13). The critical exponent for sample B is $\zeta=0.817\pm0.006$, as summarized in Table IV.

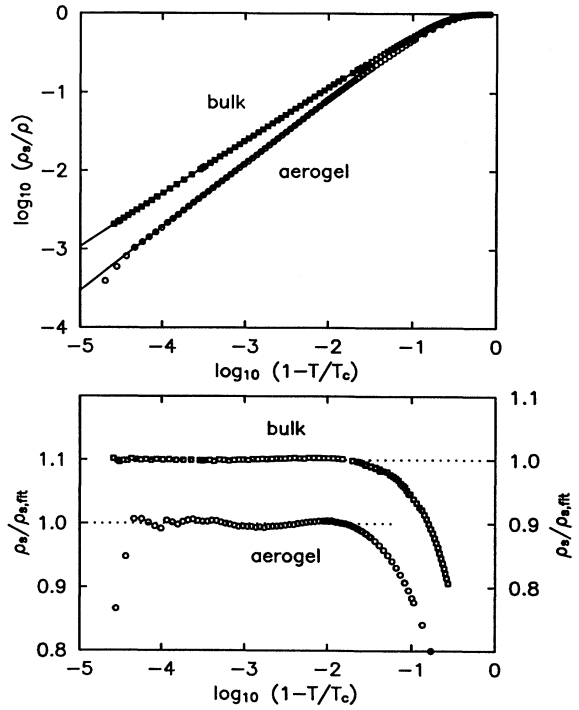

FIG. 16. This is the superfluid density power law for sample F, at saturated vapor pressure. For comparison, our aerogel data (○) are plotted alongside the bulk data (□) of Greywall and Ahlers (Ref. 13). The critical exponent for sample F is $\zeta=0.811\pm0.004$, as summarized in Table IV.

ponent, but two samples do not establish universality.

Mulders, Mehrotra, Goldner, and Ahlers[67] have done an extensive series of superfluid density measurements on the three different Airglass aerogels that we purchased. A heat pulse propagation technique was used and data were taken under a range of pressures from saturated vapor pressure (SVP) up to 29 bars. One of their three samples was cut from the same block of aerogel as our sample F and, in this case, their ρ_s measurements agreed with ours. They also saw the same residual superfluid mass decoupling between T_c and T_λ that we saw. However, they found that higher-order corrections to scaling were needed to make all of the data below T_c, especially those taken at higher pressures, collapse onto a single curve with one "universal" exponent. Their correction terms allowed them to fit their data over a wider range of reduced temperatures, $t<10^{-1}$ for them, as opposed to $t<10^{-2}$ for us. Most of the analysis was focused on just one of the three samples, the lightest one, and for that sample they obtained a pressure-independent exponent of $\zeta=0.755\pm0.003$.

B. Critical behavior in the heat capacity

On the gross temperature scale depicted in Fig. 17, the heat capacity of ^{4}He-filled aerogel looks much like the heat capacity of bulk helium. Well above T_λ, on a per mole basis, this heat capacity is essentially equal to that of bulk helium. Because this agreement was so good in sample C, where we knew very well how much helium we had put inside the cell, we assumed it to be exact in samples D and G, and used this assumption to fine tune our initial assessment of the helium dosage. Corrections of 1% or 2% were needed to account for uncertainties in the volume of the level sensor assembly. At temperatures

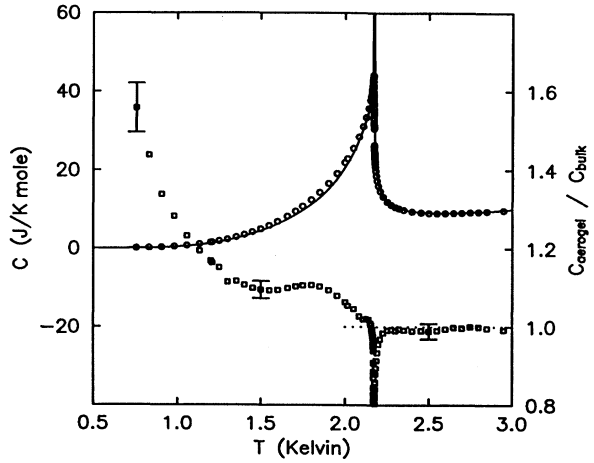

FIG. 17. The normalized heat capacity (○) for sample C is shown here on a gross temperature scale to emphasize its similarity with the bulk singularity, which is shown as a solid line (Refs. 1, 15, 69, and 70). The error bars on the ratio of these two heat capacities (□) are mostly due to uncertainties in the published data for the bulk heat capacity far from T_λ.

well below T_c, the ratio of aerogel to bulk heat capacity was clearly not one. The behavior at these two temperature extremes is understandable. Outside the critical region, heat capacities are determined by the characteristics of the low-energy excitations. Below T_c, excitations associated with the flow of superfluid helium are modified by the tortuosity of the porous structure. Above T_λ, there is of course no superflow. As the temperature decreased to zero, we found that the heat-capacity ratio stayed more or less constant until about 1.5 K, at which point it started to rise again. This is very reminiscent of the velocity of second sound in bulk helium, where a similar type of behavior was seen and attributed to a phonon-roton crossover.

To see what is happening closer to the critical regions at T_c and T_λ, consider Figs. 18 and 19. The main observation is that there are two singularities, a cusplike one associated with the superfluid transition in aerogel, and a logarithmiclike one due to the presence of bulk liquid in the fill lines and elsewhere. By "elsewhere," we mean the network of void spaces that was already postulated on the basis of the superfluid density data. An alternative explanation has been given by Machta,[68] but it does not predict the correct shape for the heat-capacity singularities. Moreover, this void signature is not present in recent heat-capacity data taken on aerogel samples grown *in situ*.[66] The amount of rounding seen at the cusplike singularity was sample dependent, but, for a given block of aerogel, the reduced temperature at which this rounding first became evident was more or less independent of the type of measurement being made, as we can see by comparing Figs. 18 and 19 with Figs. 12 and 13. Sample G was somewhat unusual in that the transition seemed to be rounded on only the high-temperature side of T_c. We are of course assuming that T_c is located at the sharp cusp, not at a point somewhere between that cusp and the inflection point approximately 200 μK higher in temperature.

Our claim that the cusplike singularity in the heat capacity is *coincident* with the superfluid transition is based on more than just an approximate agreement between the transition temperatures from the C and ρ_s measurements. Although this agreement was quite good for the Airglass aerogels, it was not so good for the DESY aerogels. Here, the T_c shifts varied from 4.0 to 5.7 mK, even though all of the samples were cut from the same block of aerogel. We suspect now that much of this variation was due to the differing amounts of compression that were used to mount the samples. To resolve this question, we modified one of our torsional oscillators to allow for a simultaneous measurement of the heat capacity. We hung the oscillator from a superleak-plugged capillary, wrapped a heater around the sample head, attached a resistance thermometer to the vibration isolator, and then cooled down. Even though there was a lot of metal in the vibration isolator structure, the total heat capacity of the filled cell was still about 22 times larger than the heat capacity of the empty cell. The cell ther-

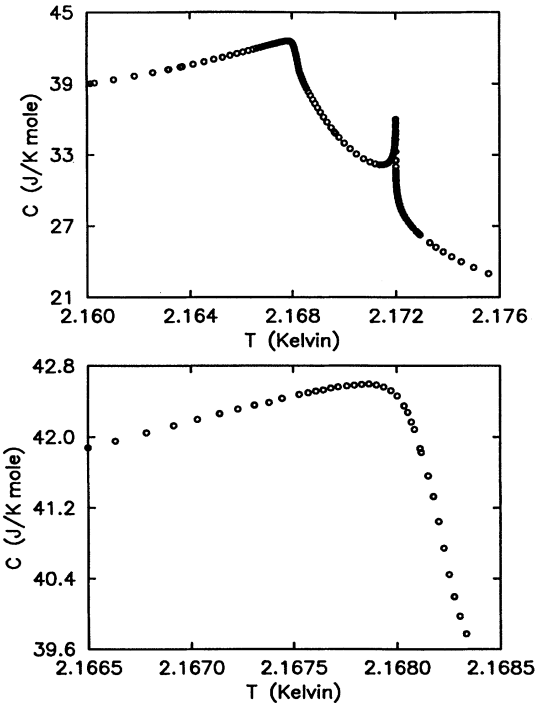

FIG. 18. This is the heat capacity for sample D, normalized by the number of moles of ^{4}He inside the cell, with no bulk correction. The bottom plot shows just how sharp the cusplike singularity really is, and it should be compared against Fig. 12.

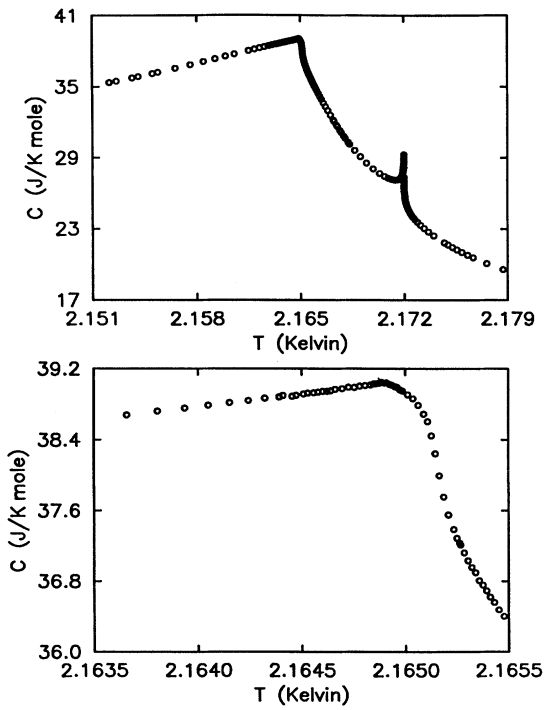

FIG. 19. This is the heat capacity for sample G, normalized by the number of moles of ^{4}He inside the cell, with no bulk correction. The bottom plot shows just how sharp the cusplike singularity really is, and it should be compared against Fig. 13.

mometer in this experiment was not very sensitive, so the heat-capacity measurements had to be done with an interleaved set of 0.44-mK temperature steps. Within the limited resolution of these large step sizes, Fig. 20 shows that the superfluid density and heat-capacity singularities are indeed coincident.

To figure out how much bulk liquid we had in our cell, we subtracted off the bulk singularity[1,15,69,70] by adjusting the scale factor until the data were as smooth as possible through T_λ. The inferior technology used on sample C made the bulk signature look more like a jump discontinuity than a logarithmic singularity. Significantly better bulk subtractions were done on samples D and G. Since the final few data points within 15 μK of T_λ were rather noisy, smeared out by temperature averaging effects, and possibly distorted by the gravitational rounding due to the 6–7 mm column of liquid in the level sensor, the optimization was performed on a subset that excluded these questionable data points. A demonstration plot is given in Fig. 21. The bulk-subtracted data are renormalized to account for the amount of ^{4}He responsible for the aerogel transition. The void fractions deduced from this procedure are listed in Table V. They are significantly larger than the void fractions deduced from the torsional oscillator data because calorimeters are sensitive to each and every void, not just the percolating network that is detected by a torsional oscillator.

For a generic superfluid density exponent of $\zeta=0.81\pm0.01$, hyperscaling predicts that the heat-capacity exponent should be $\alpha=2-d\zeta/(d-2)=-0.43\pm0.03$. Although this was clearly not an adequate description of our heat-capacity data, we decided to force a fit to a continuous cusp singularity with the hyperscaling exponent in order to see just how bad the situation was. Only sample D will be discussed in this regard as our fitting algorithms would not even converge for sample G. The resultant fit is shown in Fig. 22. The analytic background was taken to be a constant $C_{\max}$, which was adjusted along with T_c in order to obtain the optimal fit. Insofar as the critical behavior at a given t is a reflection of the structure of the aerogel impurity at the correlation length $\xi(t)$, we expect the power law to be symmetric with respect to $\xi(t)$, not with respect to t. Since from hyperuniversality we know that $\xi(t)$ scales as $[t^2C(t)]^{-1/3}$, the asymmetry in $C(t)$ with respect to the two sides of T_c ought to be, and is, reflected in an asymmetry in the range of the power-law fits. The systematic

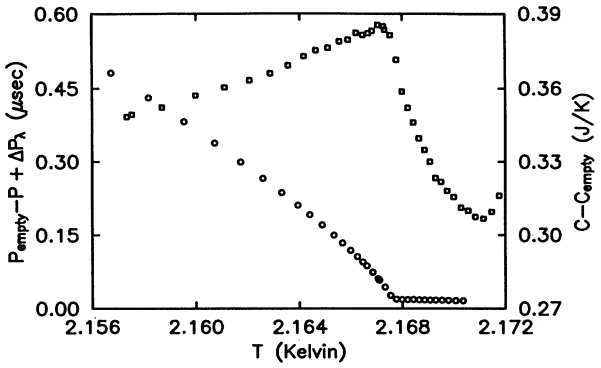

FIG. 20. The superfluid density (○) and heat capacity (□) were measured simultaneously in sample E, using interleaved 0.44-mK temperature steps. Within the resolution implied by these step sizes, the superfluid density and heat-capacity singularities appear coincident.

deviations from this power law were about 2%, nowhere near as good as with our superfluid density power laws, and nothing could be done to make the power-law fit work near the final 4 mK below T_c.

For the region closest to the transition below T_c, we found that a linear-t fit worked as well as anything else for both samples D and G, as we demonstrate in Fig. 23. Our fitting algorithm allowed both $C_{\max}$ and T_c to vary. In sample D, we found that the optimal T_c for the linear-t fit was identical to the T_c required by the hyperscaling-enforced fit, even though the optimal $C_{\max}$ was clearly very different. The systematic deviations were serious, 2% for reduced temperatures below $10^{-2.7}$ in sample D, and as much as 10% for reduced temperatures below $10^{-2.3}$ in sample G. However, recent data by Larson, Mulders, and Ahlers[71] on the isobaric thermal expansion coefficient, which can be related to the specific heat through thermodynamic arguments, confirm that this nearly linear-t behavior is real.

C. Questions of interpretation

These data demonstrate that the sharpness of the superfluid phase transition in a ^{4}He-filled porous medium does not have to have anything to do with the narrowness of the pore size distribution. In general, our Airglass samples had much sharper transitions than our DESY

TABLE V. For our heat-capacity experiments, the total helium dosage is taken to be $n_t=n_g+n_f$, where n_g is the amount inside the aerogel and n_f is the amount inside the fill lines and level sensor. In subtracting off the logarithmic singularity, we arrive at a number n_b for the total amount of bulklike liquid inside our cell. The existence of large voids within the aerogel itself was postulated because we found that $n_b > n_f$ in all cases. We have listed the bulk percentages in two ways, as a fraction n_b/n_t of all the ^{4}He inside the cell, and as a fraction $(n_b-n_f)/n_g$ of just the ^{4}He inside the aerogel.

Sample	ρ (g/cm^3)	n_t (moles)	n_g (moles)	n_b/n_t (%)	$(n_b-n_f)/n_g$ (%)
C	0.133	not applicable	0.006 92	not applicable	~16.5
D	0.133	0.026 25	0.024 65	16.84	11.43
G	0.200	0.024 80	0.023 86	10.19	6.65

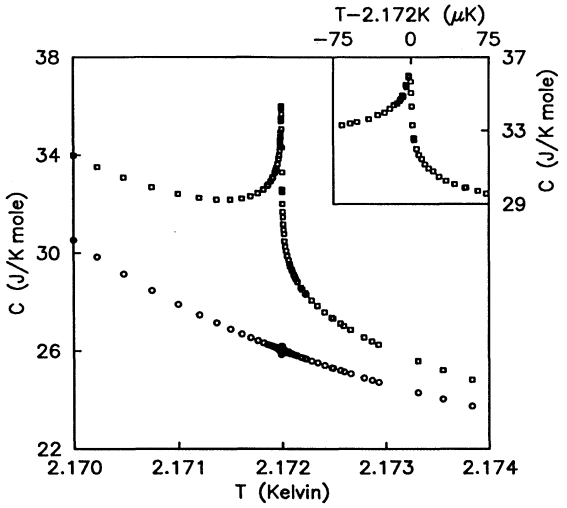

FIG. 21. The heat capacity for sample D is shown before (□) and after (○) the subtraction of a 16.84% bulk heat-capacity contribution. Depicted in the inset is a blowup of the uncorrected data near T_λ.

samples. This suggests that the DESY samples were more inhomogeneous, and we can think of two ways that this could have come about. First, these samples were known to have been exposed to ambient humidity before they were given to us, and what this exposure did to the sample homogeneity we do not know. Second, they were compression mounted, and even a little bit of friction along the sample cell walls could have led to a rather uneven compression.

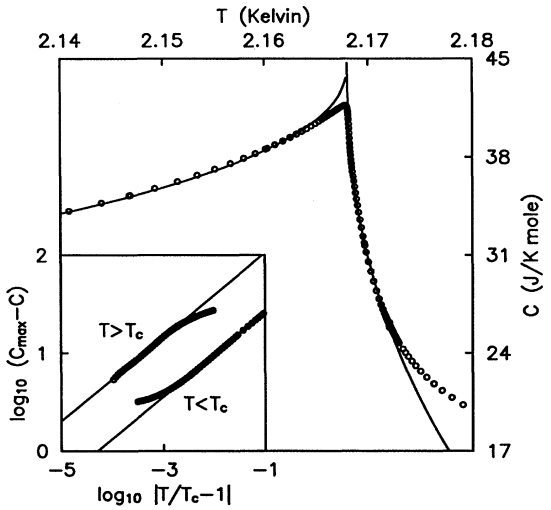

FIG. 22. This is the hyperscaling-enforced fit to the bulk-corrected heat-capacity data of sample D. The fit was to a continuous cusp singularity with a temperature-independent background, $C_{\max}=44.73$ J/K mole, and with the same exponent on both sides of T_c. Below the transition, we got a singular contribution of $69.85|t|^{0.43}$ for $|t|$ from 10^{-1} to $10^{-2.7}$, as opposed to $283.5|t|^{0.43}$ for $|t|$ from 10^{-3} to 10^{-4} above the transition. For clarity, the data closest to T_c are deleted in the $\log_{10}$-$\log_{10}$ plot inset.

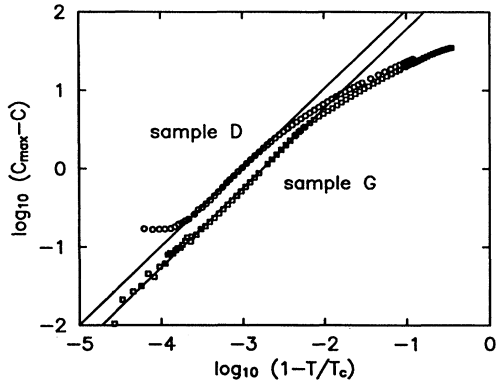

FIG. 23. Nearly linear-t behavior was observed in the heat capacity just below T_c. These fits were done to the bulk-corrected data of samples D and G, with $C_{\max}=41.84$ and 38.46 J/K mole, respectively. The quality of the power-law fit was not significantly improved by allowing for an exponent different from one.

As a first step, we want to know if the critical exponents can be computed from what little we know about the structure of the aerogel backbone. Weinrib and Halperin's theory makes a specific prediction, but we are not certain that it is applicable. Within the framework of the magnetic phase transitions that they envisioned, it is obvious that the local T_c's should scale with the local impurity concentration because impurities weaken the strength of the locally averaged magnetic interaction. It is not at all obvious to us that the same connection can be made for ^{4}He-filled porous media, but suppose for the moment that it can. Scattering experiments on a variety of aerogels[22,46] suggest that the backbone structure might be describable by fractal exponents ranging from 2.1 up to 2.4, so the most naive application of this theory predicts $\zeta_{\text{impure}}=2/(d-D_f)=3.3$ to 2.2, which clearly differs from the measured values. The disagreement may be moot for a number of reasons. First, the correlation lengths that are deduced from our superfluid density power-law fits, as listed in Table IV, extend out to much longer length scales than the cluster sizes that are determined from the scattering data. For aerogels with densities of 0.133 and 0.200 g/cm^3, the fractal regimes broke down at 21.1 and 10.6 nm, respectively, but our superfluid density power laws extended out to 304 and 989 nm (samples B and F). Moreover, our aerogels were base-catalyzed and probably not describable by a single fractal exponent. Weinrib and Halperin's theory also assumed a Gaussian distribution of local T_c. The half-width of this Gaussian must be less than $T_\lambda - T_c$ because impurities can only depress the local T_c, never increase it. However, the observed critical behavior was clearly being affected at temperatures well beyond the half-width of this Gaussian on the low-temperature side of T_c, which suggests that an asymmetric local T_c distribution may be more appropriate.[72]

Another school of thought asserts that we are not yet close enough to the critical point to observe the true critical exponents. Indeed, Weinrib and Halperin's theory is expected to be applicable only at reduced temperatures

that are much smaller than the reduced T_c shift. The more serious problem in this regard arises from the fact that superfluid ^{4}He is only marginally stable against disorder of the Harris type because α_{pure} is only slightly negative. Even in the case of short-range or uncorrelated disorder, there can be slow transients in the critical behavior, leading to effective exponents that are quite different from the true critical exponents. In the theory of Narayan and Fisher,[73] the correction terms can be adjusted to give an effective superfluid density exponent of 0.836 to 0.791 over reduced temperatures of 10^{-2} to 10^{-4}. This may not seem like such a bad fit at first, but the corresponding prediction for the effective heat-capacity exponent is -0.180 to -0.135, in serious disagreement with our data. We acknowledge that one of our most striking observations, the failure of hyperscaling, is consistent with the supposition that we are not yet in the asymptotic regime. However, none of our data show even the slightest inclination toward bulklike behavior as $t \rightarrow 0$. For the heat capacity below T_c, the critical behavior seems to be veering farther and farther away from bulklike behavior. To suggest that we need to get even closer to T_c than we already have, in order to observe the "real" critical behavior, is as much a reflection of the limits of the existing theory as a critique of the aerogel system. Ultimately, the marginality issue may have to be settled by doing a similar set of experiments on a system in which α_{pure} is more strongly negative, such as a 3D Heisenberg ferromagnet.

There is another reason why hyperscaling might not work. Superfluid density and heat-capacity measurements do not probe exactly the same body of liquid.[74] Torsional oscillators probe only the percolating body of liquid within a viscous penetration depth of the aerogel substrate, which is an idealized subset of the complete system. In contrast, adiabatic calorimeters probe all of the liquid. The net result is that heat capacities may be more sensitive to nonidealities such as the aerogel cluster size. When we compute the reduced temperatures at which the correlation lengths become comparable to the cluster sizes extracted from the scattering data, 5.1×10^{-3} and 1.34×10^{-2} for our representative 0.133 and 0.200 g/cm^3 aerogels, we find that they are in the same general vicinity as the break in the heat-capacity data where the linear-t behavior begins. The superfluid density may not be affected by this cluster size limit because the dynamics of the oscillator experiment select out a *larger* percolating body of liquid. We note that there has been some recent work on the issue of connectivity in aerogel.[75]

In spite of our failure to understand the critical exponents, we believe that we have a qualitative explanation for why ^{4}He-filled aerogel has an observable heat-capacity singularity, while ^{4}He-filled Vycor does not. The argument depends on a *coarse-grain averaged* interpretation of hyperuniversality. We will offer two explanations. Renormalization group calculations account for spatial fluctuations of the order parameter on all length scales up to the correlation length, but they produce a spatially independent result in the end. This is because, implicit in the theory, there is an assumption of macroscopic homogeneity on length scales much larger than the attainable correlation lengths. This can happen only if we treat the porous glass as an effective medium and coarse-grain average all of the thermodynamic quantities that go into the theory. Alternatively, recall that hyperuniversality is derived by considering the singular part of the free energy inside a correlation volume. The correlation length is derived by considering the free energy due to a twist in the phase of the order parameter, where the order parameter itself is definable only over a correlation volume. So the index of refraction correction, $1-\chi_m = n^{-2}$, that appears in Eq. (34) is just a reflection of the fact that energies defined over length scales as large as the divergent correlation length are transported at the group velocity. The porosity correction is needed because, in an impurity interpretation, the "sample" volume includes both the helium and the aerogel.

To predict the size of the heat-capacity singularity from the critical amplitude $\tilde{\rho}_{s_0}$ for that system, we must first locate another system in the *same* universality class for which both ρ_s and C have previously been measured. Vycor is an easy case because it is bulklike. Coarse-grain averaging brings $\tilde{\rho}_{s_0}$ down to 0.010 g/cm^3, versus 0.351 g/cm^3 for bulk helium. Hyperuniversality, given by Eq. (12), thus predicts a heat-capacity singularity for ^{4}He-filled Vycor that is only 0.04% of the background at a reduced temperature of $10^{-2.5}$, much too small to have been seen in any of the previous experiments. We note that in the case of thin films adsorbed on the surface of Vycor, coarse-grain averaging arguments have successfully predicted the size of the observed heat capacity singularity.[29] Strictly speaking, in order to predict the size of the heat-capacity singularity in ^{4}He-filled aerogel, we must first have prior knowledge of some other member of this new universality class (we are taking for granted that such a class exists). No such knowledge exists, but if we assume that the dimensionless universal constant X is always of order unity, then we can see why the heat-capacity singularity in ^{4}He-filled aerogel is observable—$\tilde{\rho}_{s_0}$ is not very different from that seen in bulk helium. Specifically, it was 0.418 and 0.374 g/cm^3 for samples B and F. We note that the hyperscaling-enforced fit to sample D gave $X=1.9$, which is rather close to unity.

If we take the agreement between the measured superfluid density exponents to mean that our two representative aerogels are in the same universality class, then we can predict that the heat-capacity singularity per unit volume in sample D should be 1.25–1.40 times bigger than that in sample G. In practice, the failure of hyperscaling means that X is no longer temperature independent and consequently, as we show in Fig. 24, neither is the heat-capacity ratio. What is curious, however, is that there is a small range of reduced temperatures, at 10^{-2} below T_c, where this heat-capacity ratio flattens out *at the predicted value.* One might be tempted to believe that the scaling theory is correct after all, and that it breaks down only because the ρ_s and C measurements no longer probe the same body of liquid once the correlation length exceeds the aerogel cluster size. However, this argument is not self-consistent because the particular

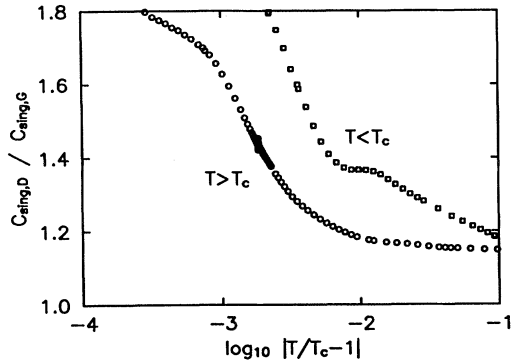

FIG. 24. Hyperuniversality predicts that the singular part of the heat capacity *per unit volume* should be 1.25–1.40 times larger in sample D than in sample G. We define the singular component as $C_{sing}(t)=C_{max}-C(t)$, where $C(t)$ is the bulk-corrected heat capacity and C_{max} is the peak height obtained from a fit to the linear-t region (which is not equivalent to the peak height given by the hyperscaling-enforced fit).

choice of C_{max} that was used here does not yield the hyperscaling exponent over any appreciable range of reduced temperatures, let alone the region of interest near 10^{-2} below T_c.

Although our ^{4}He-filled aerogels have not shown much variation in their critical behavior, other groups working with other aerogel samples have found slightly different results. If there is a trend, it is that the least dense aerogels have the smallest T_c shifts and the smallest ρ_s exponents, $\zeta=0.77$ in the case of a 98% porous aerogel recently studied by Ma and Chan.[66] For one particularly dense 85% porous aerogel,[76,66] the ρ_s exponent was 0.95 and *no singularity was found in the heat capacity.* In fact, the heat capacity had a broad maximum at a temperature somewhat higher than the superfluid transition, exactly as had been seen in the older Vycor and xerogel samples. Pessimists might be inclined to dismiss these kinds of experiments as being too specific to the particular aerogel under study, with different answers arising for each and every sample. To some extent, this is true. What we have learned so far suggests that particular attention will have to be paid to the many different length scales that are involved: the correlation length for fluctuations of the order parameter, the range of length scales characterizing the aerogel glass, and the viscous penetration depth in our oscillator experiments. This makes the problem more difficult, but not necessarily insurmountable. Similar issues arise in the study of electron transport in mesoscopic scale conductors[77] and universal behavior in the amplitude of the aperiodic conductance fluctuations has already been discovered. It might therefore be interesting to see if any aspect of this new critical behavior that we observe in the ^{4}He-filled aerogel system is invariant against changes in the sample under study. Failing that, one might at least like to know how the critical behavior is related to some *measurable* characterization of the disordered structure. This is the direction in which we hope the research will ultimately progress.

D. Possible dynamical effects

We present evidence here for the existence of a coincident thermal conductivity singularity at the superfluid transition. Some of the raw $T(t)$ data from the heat-capacity experiment on sample D are shown in Fig. 25. In the bulk helium experiments, Ahlers[15] observed that his $T(t)$ exhibited a noticeable overshoot as soon as the cell temperature crossed over T_λ. Above T_λ, the heat pulse was not able to diffuse through the liquid quickly enough to prevent the thermometer from overheating. We saw this same effect at T_λ in our cell. However, we also saw a similar but much less dramatic effect at T_c. The 2-μK temperature steps we took near T_λ used heater powers of 34 nW. For this demonstration, we used large 100-μK steps near T_c with heater powers of 1.6 μW. To maintain the same vertical scale as the T_λ plot, we shifted the data so that only the points taken after the heater was turned off appear on this plot. The numbers printed atop each curve specify $T-T_c$ at the end of the heater pulse. In spite of the fact that we were putting in a lot more energy at a much higher rate, the overshoot did not appear until we were 1 mK above T_c. This meant that there was still a lot of thermal conduction in our sample at $\frac{1}{2}$ mK above T_c, well beyond even the inflection point in the heat capacity.

Something is giving us a large thermal conduction above T_c. What is the underlying mechanism? Critical

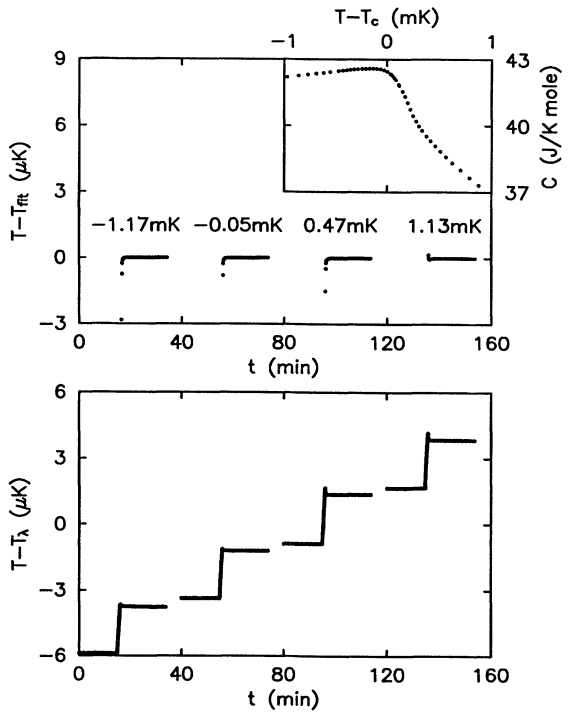

FIG. 25. Overshoot signals in the raw $T(t)$ data from sample D are suggestive of a singularity in the thermal conductivity, as described in the text. The numbers above each of the four curves in the top figure indicate the value of $T-T_c$ just after the heater was turned off, showing clearly that the tiny overshoot at T_c is not associated with the $C(T)$ inflection point emphasized in the inset.

point fluctuations are one possibility, but first we must eliminate the more straightforward case of a counterflow mechanism. We know that the superfluid can flow through the aerogel, but the normal fluid is supposed to be viscously locked to the porous substrate. Normal fluid counterflow is still possible, however, through cracks along the sample edges. This gives us a conduction mechanism that shuts off above T_c, if we ignore the counterflow contained entirely within the cracks, and it is inconsistent with our $T(t)$ data. Direct measurements of the thermal conductivity may therefore prove very interesting.

ACKNOWLEDGMENTS

The work reported here was supported by the National Science Foundation through Grant No. NSF-DMR-8418605 and by the Cornell Materials Science Center through Grant No. NSF-DMR-8818558. G.K.S.W. acknowledges financial support from the Natural Sciences and Engineering Research Council of Canada. P.A.C. acknowledges financial support from AT&T Bell Laboratories. The DESY aerogel sample was donated by G. Poelz. We thank N. Mulders and J. R. Beamish for bringing the epoxy mentioned in Ref. 34 to our attention. Portions of the torsional oscillator were fabricated by S. Murphy. The TOADS box was designed and built by P. Moster and D. McQueeney. CAB salt crystals were provided by R. Duncan and G. Ahlers. W. Ho gave us a complete LSI-11/73 computer system. We thank A. J. Hunt of Lawrence Berkeley Laboratory for providing us with the photograph depicted in Fig. 3. We are also grateful to M. H. W. Chan, M. E. Fisher, J. M. Parpia, and E. D. Siggia for their comments on this work.

*Present address: Division of Physics, Mathematics and Astronomy, California Institute of Technology, Pasadena, California 91125.

[1]J. A. Lipa and T. C. P. Chui, Phys. Rev. Lett. **51**, 2291 (1983); (unpublished).

[2]For example, see G. Ahlers, Rev. Mod. Phys. **52**, 489 (1980); in *The Physics of Liquid and Solid Helium, Part I,* edited by K. H. Bennemann and J. B. Ketterson (Wiley, New York, 1976), p. 85.

[3]K. G. Wilson, Rev. Mod. Phys. **47**, 773 (1975); K. G. Wilson and J. B. Kogut, Phys. Rep. C **12**, 75 (1974).

[4]For example, see M. E. Fisher, Rev. Mod. Phys. **46**, 597 (1974); in *Critical Phenomena,* edited by F. J. W. Hahne, Lecture Notes in Physics Vol. 186 (Springer-Verlag, Berlin, 1983), p. 1; L. P. Kadanoff, in *Phase Transitions and Critical Phenomena,* edited by C. Domb and M. S. Green (Academic, London, 1976), Vol. 5A, p. 1.

[5]M. R. Moldover, J. V. Sengers, R. W. Gammon, and R. J. Hocken, Rev. Mod. Phys. **51**, 79 (1979); M. F. Collins, *Magnetic Critical Scattering* (Oxford University Press, New York, 1989).

[6]A. B. Harris, J. Phys. C **7**, 1671 (1974).

[7]A. B. Harris and T. C. Lubensky, Phys. Rev. Lett. **33**, 1540 (1974); T. C. Lubensky, Phys. Rev. B **11**, 3573 (1975); G. Grinstein and A. Luther, *ibid.* **13**, 1329 (1976).

[8]J. M. Hastings, L. M. Corliss, and W. Kunnmann, Phys. Rev. B **31**, 2902 (1985); R. J. Birgeneau, R. A. Cowley, G. Shirane, H. Yoshizawa, D. P. Belanger, A. R. King, and V. Jaccarino, *ibid.* **27**, 6747 (1983); R. A. Dunlap and A. M. Gottlieb, *ibid.* **23**, 6106 (1981).

[9]A. B. Weinrib and B. I. Halperin, Phys. Rev. B **27**, 413 (1983).

[10]M. H. W. Chan, K. I. Blum, S. Q. Murphy, G. K. S. Wong, and J. D. Reppy, Phys. Rev. Lett. **61**, 1950 (1988). In Table I, the scale for ρ_{s_0} should be 10^{-2} g/cm^3.

[11]G. K. S. Wong, P. A. Crowell, H. A. Cho, and J. D. Reppy, Phys. Rev. Lett. **65**, 2410 (1990).

[12]*Aerogels: Proceedings of the First International Symposium,* edited by J. Fricke (Springer-Verlag, Berlin, 1986).

[13]D. S. Greywall and G. Ahlers, Phys. Rev. A **7**, 2145 (1973).

[14]A. Singsaas and G. Ahlers, Phys. Rev. B **30**, 5103 (1984).

[15]G. Ahlers, Phys. Rev. A **3**, 696 (1971).

[16]J. C. Le Guillou and J. Zinn-Justin, Phys. Rev. B **21**, 3976 (1980); D. Z. Albert, *ibid.* **25**, 4810 (1982).

[17]B. D. Josephson, Phys. Lett. **21**, 608 (1966).

[18]M. E. Fisher, M. N. Barber, and D. Jasnow, Phys. Rev. A **8**, 1111 (1973).

[19]P. C. Hohenberg, A. Aharony, B. I. Halperin, and E. D. Siggia, Phys. Rev. B **13**, 2986 (1976); D. Stauffer, M. Ferer, and M. Wortis, Phys. Rev. Lett. **29**, 345 (1972).

[20]G. Grinstein, in *Fundamental Problems in Statistical Mechanics,* edited by E. G. D. Cohen (North-Holland, Amsterdam, 1985), Vol. VI, p. 147; D. S. Fisher, G. Grinstein, and A. Khurana, Phys. Today **41** (12), 56 (1988).

[21]B. M. McCoy and T. T. Wu, Phys. Rev. **176**, 631 (1968).

[22]R. Vacher, T. Woignier, J. Pelous, and E. Courtens, Phys. Rev. B **37**, 6500 (1988).

[23]D. W. Schaefer and K. D. Keefer, Phys. Rev. Lett. **56**, 2199 (1986).

[24]G. Ahlers, J. Low Temp. Phys. **1**, 159 (1969); M. Kriss and I. Rudnick, *ibid.* **3**, 339 (1970).

[25]V. L. Ginzburg and L. P. Pitaevskii, Zh. Eksp. Teor. Fiz. **34**, 1240 (1958) [Sov. Phys. JETP **7**, 858 (1958)]; Yu. G. Mamaladze, *ibid.* **52**, 729 (1967) [*ibid.* **25**, 479 (1967)].

[26]W. Huhn and V. Dohm, Phys. Rev. Lett. **61**, 1368 (1988).

[27]C. W. Kiewiet, H. E. Hall, and J. D. Reppy, Phys. Rev. Lett. **35**, 1286 (1975); J. E. Berthold, D. J. Bishop, and J. D. Reppy, *ibid.* **39**, 348 (1977).

[28]R. A. Joseph and F. M. Gasparini, in *Proceedings of LT-15* [J. Phys. (Paris) Colloq. **39**, C6-310 (1978)]; D. F. Brewer, J. Low Temp. Phys. **3**, 205 (1970).

[29]D. Finotello, K. A. Gillis, A. Wong, and M. H. W. Chan, Phys. Rev. Lett. **61**, 1954 (1988); M. H. W. Chan, in *Proceedings of LT-19,* edited by D. S. Betts [Physica B **169**, 135 (1991)].

[30]M. W. Shafer, D. D. Awschalom, J. Warnock, and G. Ruben, J. Appl. Phys. **61**, 5438 (1987).

[31]J. M. Kosterlitz and D. J. Thouless, J. Phys. C **6**, 1181 (1973); J. M. Kosterlitz, *ibid.* **7**, 1046 (1974).

[32]Airglass AB, Box 150, S-245 00 Staffanstorp, Sweden.

[33]G. A. Nicolaon and S. J. Teichner, Bull. Soc. Chim. Fr. **5**, 1906 (1968).

[34]BIPAX Tra-Bond BA-2151 epoxy is manufactured by TRA-CON, Inc., Resin Systems Division, 55 North Street, Medford, MA 02155.

[35]R. K. Iler, *The Chemistry of Silica: Solubility, Polymerization, Colloid and Surface Properties, and Biochemistry* (Wiley, New

York, 1979).
[36]G. Poelz and R. Riethmüller, Nucl. Instrum. Methods **195**, 491 (1982).
[37]S. Henning and L. Svensson, Phys. Scr. **23**, 697 (1981).
[38]G. Schuck and W. Dietrich, in *Aerogels: Proceedings of the First International Symposium,* edited by J. Fricke (Springer-Verlag, Berlin, 1986), p. 148.
[39]P. H. Tewari, A. J. Hunt, J. G. Lieber, and K. Lofftus, in *Aerogels: Proceedings of the First International Symposium,* edited by J. Fricke (Springer-Verlag, Berlin, 1986), p. 142.
[40]P. Meakin, in *Phase Transitions and Critical Phenomena,* edited by C. Domb and J. L. Lebowitz (Academic, London, 1988), Vol. 12, p. 335.
[41]B. B. Mandelbrot, *The Fractal Geometry of Nature* (Freeman, New York, 1983).
[42]T. A. Witten and L. M. Sander, Phys. Rev. Lett. **47**, 1400 (1981).
[43]P. Meakin, Phys. Rev. A **27**, 604 (1983); **27**, 1495 (1983).
[44]P. Meakin, Phys. Rev. Lett. **51**, 1119 (1983); M. Kolb, R. Botet, and R. Jullien, *ibid.* **51**, 1123 (1983).
[45]R. Jullien, M. Kolb, and R. Botet, J. Phys. (Paris) Lett. **45**, L211 (1984); M. Kolb and R. Jullien, *ibid.* **45**, L977 (1984); R. Jullien and M. Kolb, J. Phys. A **17**, L639 (1984).
[46]F. Ferri, B. J. Frisken, and D. S. Cannell, Phys. Rev. Lett. **67**, 3626 (1991).
[47]P. Levitz, G. Ehret, S. K. Sinha, and J. M. Drake, J. Chem. Phys. **95**, 6151 (1991); see also Phys. Today **42** (7), 25 (1989).
[48]P. Wiltzius, F. S. Bates, S. B. Dierker, and G. D. Wignall, Phys. Rev. A **36**, 2991 (1987); D. W. Schaefer, B. C. Bunker, and J. P. Wilcoxon, Phys. Rev. Lett. **58**, 284 (1987).
[49]J. W. Cahn, J. Chem. Phys. **42**, 93 (1965).
[50]G. K. S. Wong, in *Experimental Techniques in Condensed Matter Physics at Low Temperatures,* edited by R. C. Richardson and E. N. Smith (Addison-Wesley, Redwood City, 1988), p. 187. On p. 196, the equation for the torsional spring constant due to the dc bias voltage should be $K=-CV_0^2(r/d)^2$.
[51]P. M. Morse, *Vibration and Sound* (McGraw-Hill, New York, 1948), p. 398.
[52]K. A. Shapiro and I. Rudnick, Phys. Rev. **137**, A1383 (1965).
[53]M. J. McKenna, T. Slawecki, and J. D. Maynard, Phys. Rev. Lett. **66**, 1878 (1991).
[54]G. Agnolet, D. F. McQueeney, and J. D. Reppy, Phys. Rev. B **39**, 8934 (1989).
[55]D. F. McQueeney, Ph.D. thesis, Cornell University, 1988, Appendix F.
[56]J. B. Mehl and W. Zimmerman, Phys. Rev. **167**, 214 (1968).
[57]A. W. Yanof and J. D. Reppy, Phys. Rev. Lett. **33**, 631 (1974); D. J. Bergman, B. I. Halperin, and P. C. Hohenberg, Phys. Rev. B **11**, 4253 (1975).
[58]A. L. Fetter, J. Low Temp. Phys. **16**, 533 (1974).
[59]J. R. Pellam, Phys. Rev. **99**, 1327 (1955).
[60]R. P. Feynman, Phys. Rev. **94**, 262 (1954).
[61]G. K. S. Wong, Ph.D. thesis, Cornell University, 1990, Chap. 4.
[62]J. A. Lipa, B. C. Leslie, and T. C. Wallstrom, in *Proceedings of LT-16,* edited by W. G. Clark [Physica B **107**, 331 (1981)]; T. C. P. Chui and J. A. Lipa, in *Proceedings of LT-17,* edited by U. Eckern, A. Schmid, W. Weber, and H. Wühl (North-Holland, Amsterdam, 1984), p. 931; D. Marek, in *Proceedings of LT-18,* edited by Y. Nagaoka [Jpn. J. Appl. Phys. Suppl. **26**-3, 1683 (1987)].
[63]A. R. Miedema, R. F. Wielinga, and W. J. Huiskamp, Physica **31**, 1585 (1965); R. F. Wielinga and W. J. Huiskamp, *ibid.* **40**, 602 (1969); L. J. de Jongh, A. R. Miedema, and R. F. Wielinga, *ibid.* **46**, 44 (1970).
[64]Biomagnetic Technologies Inc., 4174 Sorrento Valley Blvd., P.O. Box 210079, San Diego, CA 92121.
[65]J. Zimmermann and G. Weber, Phys. Rev. Lett. **46**, 661 (1981).
[66]J. Ma and M. H. W. Chan (private communication).
[67]N. Mulders, R. Mehrotra, L. S. Goldner, and G. Ahlers, Phys. Rev. Lett. **67**, 695 (1991).
[68]J. Machta, Phys. Rev. Lett. **66**, 169 (1991).
[69]M. J. Buckingham and W. M. Fairbank, in *Progress in Low Temperature Physics,* edited by C. J. Gorter (North-Holland, Amsterdam, 1961), Vol. III, p. 80.
[70]J. Wilks, *The Properties of Liquid and Solid Helium* (Oxford University Press, New York, 1967).
[71]M. Larson, N. Mulders, and G. Ahlers, Phys. Rev. Lett. **68**, 3896 (1992).
[72]D. A. Huse (private communication).
[73]O. Narayan and D. S. Fisher, Phys. Rev. B **42**, 7869 (1990).
[74]P. G. de Gennes (private communication).
[75]D. W. Schaefer, C. J. Brinker, D. Richter, B. Farago, and B. Frick, Phys. Rev. Lett. **64**, 2316 (1990).
[76]J. R. Beamish and N. Mulders, in *Quantum Fluids and Solids–1989 (Gainesville, FL, 1989),* Proceedings of a Conference on Quantum Fluids and Solids, edited by G. G. Ihas and Y. Takano, AIP Conf. Proc. No. 194 (AIP, New York, 1989), p. 182.
[77]S. Washburn and R. A. Webb, Adv. Phys. **35**, 375 (1986); R. A. Webb and S. Washburn, Phys. Today **41** (12), 46 (1988); B. L. Al'tshuler and P. A. Lee, *ibid.* **41** (12), 36 (1988).

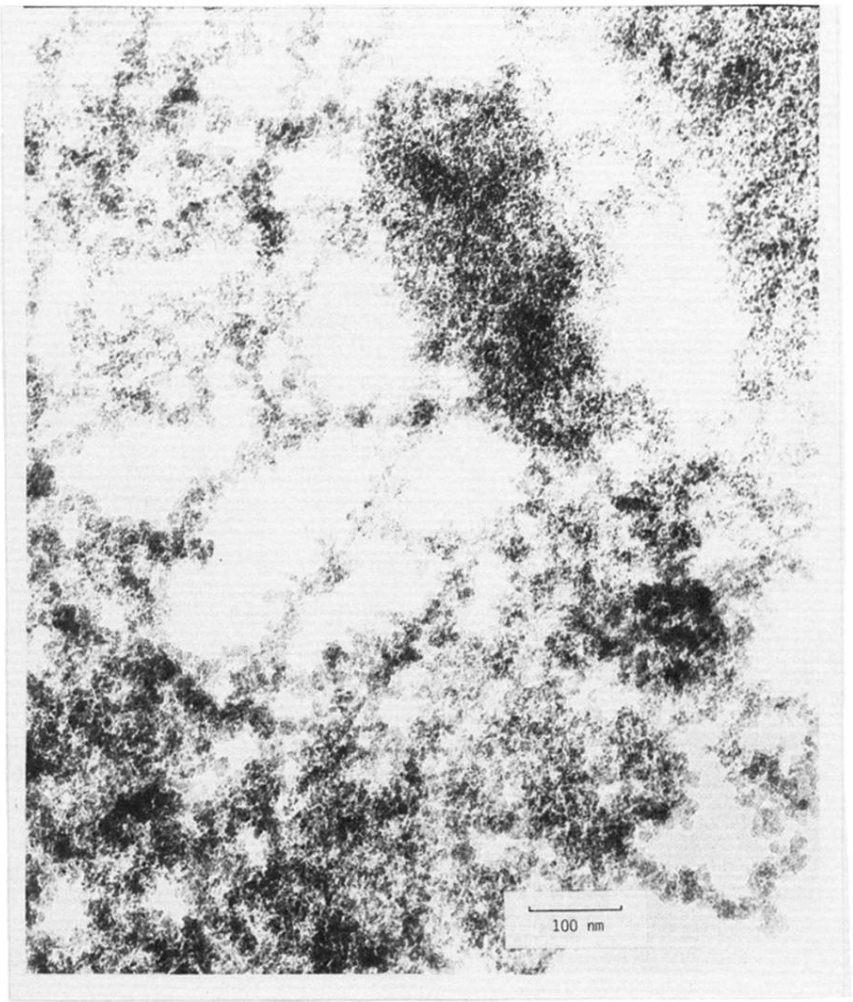

FIG. 3. This transmission electron micrograph of a carbon-coated flake of base-catalyzed aerogel was produced by Tewari, Hunt, Lieber, and Lofftus (Ref. 39). The pore space is shown in white and the scale bar at the bottom corresponds to a length of 100 nm.